

Content

Résumé.....	II
Abstract.....	V
Acknowledgment	VIII
List of Table	I
List of Figure.....	I
1 Introduction.....	1
1.1 Definition of problem	1
1.2 Objective.....	4
2 Literature review	5
2.1 Elevated temperature applications of aluminum alloys	5
2.2 Al-Mn 3xxx alloys	7
2.2.1 The effect of alloying elements.....	9
2.2.2 The evolution of constituent particles during heat treatment.....	13
2.2.3 Dispersoid particles and their evolution in Al-Mn-Si 3xxx alloys	16
2.3 Effects of Mo addition on properties	26
3 Experimental procedure	31

3.1 Alloy preparation.....	31
3.2 Heat treatments.....	32
3.3 Microstructure observation.....	34
3.4 Electrical conductivity.....	38
3.5 Microhardness.....	39
3.6 Mechanical properties test.....	40
4. Results and Discussion.....	42
4.1 Effect of Mo additions on as-cast properties.....	42
4.1.1 Microstructure.....	42
4.1.2 Microhardness and electrical conductivity.....	48
4.2 Evolution of microstructure and properties during heat treatment.....	51
4.2.1 Microstructure evolution during precipitation treatment.....	53
4.2.2 Effect of Mo on the evolution of properties during precipitation treatments.....	64
4.2.3 Effect of precipitation treatment parameters on the evolution of properties.....	69
4.3 Creep resistance and long-term thermal stability.....	81
4.4 Preheating treatment.....	87
5. Conclusions.....	92

Reference95

List of Table

Table 2.1 Tensile properties of Al-Fe-Ce and Al-Fe-V-Si alloys[26]	7
Table 2.2 Composition limits of 3004 alloys[1]	9
Table 3.1 Chemical compositions of the experimental alloys	31
Table 3.2 Heat Treatment Conditions in present project.....	33

List of Figure

Fig. 2.1 Al-Mn phase diagram[2].....	10
Fig. 2.2 Al-Mg phase diagram[2].....	11
Fig. 2.3 Back scatter electron SEM images of primary particles (a) in the as-cast state.	13
Fig. 2.4 Fraction of α -Al(Mn,Fe)Si in total amount of primary particles[30]	14
Fig. 2.5 Back scatter SEM image revealing the eutectoid transformation of the primary particles $Al_6(Mn, Fe)$ into α -Al(Mn,Fe)Si[31].....	15
Fig. 2.6 TEM image (a) and size distribution (b) of dispersoids after 24h annealing at 375 °C.[9].....	17
Fig. 2.7 The stress-strain curve of the annealed specimen and the homogenized specimen. [9].....	18
Fig. 2.8 True stress-strain curve (a) and YS at both RT and 300 °C and differernt treatment conditions (b) for AA3004 alloy[11]	19

Fig. 2.9 Evolution of EC and hardness (a) and YS (b) during a long thermal holding[11]	19
Fig. 2.10 Electrical conductivity evolution of 3003 alloy during heat treatment.[5].....	20
Fig. 2.11 TEM morphology of dispersoids precipitated during heating in 3003 alloy. (a) 350 °C (b) 400 °C (c) 500 °C (d) 580 °C [5]	21
Fig. 2.12 Size and number density evolution of dispersoids during heating in 3003 alloy.[5]	22
Fig. 2.13 SEM images which show the location of dispersoids[31].....	23
Fig. 2.14 Formation of DFZ in AA3004 alloy treated at 425 °C for 48h: (a)OM and (b)SEM, an enlargement of (a).[11].....	25
Fig. 2.15 (a)Al–Mo binary phase diagram and (b) enlarged view of the Al-rich corner (calculated using FactSage software).[23].....	27
Fig. 2.16 (a) Bright field TEM micrograph showing the Al–(Fe,Mo)–Si dispersoids in the intradendritic regions of the Mo-containing Al-Si cast alloy formed after 10h of solution treatment at 540 °C. (b) Back scattered SEM micrographs showing the solution treated (4h at 500 °C and 10h at 540 °C) microstructures of the Mo-containing Al-Si cast alloy[23].	28
Fig. 2.17 Tensile properties of the alloys at 300 °C. Solution treated at 540 °C for 10h, aged at 200 °C. For 5h and soaked at 300 °C for 100h[23].(MG3R3M alloy is made by	

adding 0.3% Mo addition into MG3R alloy).....	28
Fig. 2.18 EDS elemental line scanning across a dendrite cell showing the concentration gradients of Mo and Mn (microsegregation) in the as-cast Al-7Si-0.5Cu-0.3Mg-0.1Fe-0.3Mo-1.5Mn alloy.[24]	29
Fig. 2.19 Average dispersoid size and the number of dispersoid per unit area of the α – AlFe, Mn, MoSi in Al-7Si-0.5Cu-0.3Mg-0.1Fe-0.3Mo-1.5Mn alloy.[24]	29
Fig. 3.1 Electrical resistance furnace	32
Fig. 3.2 Electrically resistance air-circulating chamber furnace.....	33
Fig. 3.3 Optical microscope	35
Fig. 3.4 JSM-6480LV Scanning Electron Microscope	36
Fig. 3.5 JEM-2100 Transmission Electron Microscope.....	36
Fig. 3.6 Struers TegraPol-35 Grinder-Polisher.....	37
Fig. 3.7 Portable FISCHER SIGMASCOPE® SMP 10 Electrical Conductivity Measurement System	38
Fig. 3.8 NG-1000 CCD microhardness test machine	39
Fig. 3.9 Gleeble 3800 machine	41
Fig. 4.1 As-cast microstructure of (a) the base 3004 alloy; (b) M10; (c) M20; (d) M30; (e) M40; (f) M50; (g) M70	44
Fig. 4.2 SEM image of the base 3004 alloy (a-b) and SEM-EDS results(c-d)	45

Fig. 4.3 SEM image of (a)M30 and (b)M40 SEM-EDS results (c) for Mo-containing particles	47
Fig. 4.4 Optical Microstructure of M50 alloy (a) As-cast; (b) 600°C× 24h	48
Fig. 4.5 Electrical conductivity of as-cast alloys	50
Fig. 4.6 Microhardness of as-cast alloys.....	50
Fig. 4.7 Microstructure evolution during precipitation treatment for base 3004 alloy (a) 375°C/2h; (b) 375°C/8h;(c) 375°C/24h; (d)550°C/2h; (e) 550°C/8h (f) 550°C/24h, etched with 0.5%HF for 30s.	53
Fig. 4.8 Microstructure evolution of base 3004 alloy for different precipitation temperatures, etched with 0.5%HF for 30s.....	56
Fig. 4.9 Microstructure evolution of M30 alloy for different precipitation temperatures, etched with 0.5%HF for 30s.	59
Fig. 4.10 The SEM image of the dispersoids of (a) base 3004 alloy and (b) M30 alloy after treated at 550°Cfor 24 hours	61
Fig. 4.11 TEM-EDS spectrum of the dispersoids in M30 alloy after treated at 550°C for 12 hours.....	62
Fig. 4.12 Area percentage of DFZ after 24 hours precipitation treatment at different temperatures.....	63
Fig. 4.13 Evolution of (a)electrical conductivity, and (b) microhardness for alloys with	

different Mo additions during precipitation treatment at 375°C	65
Fig. 4.14 Evolution of electrical conductivity (a) and microhardness (b) for alloys with different Mo additions during precipitation treatment at 550°C.....	66
Fig. 4.15 YS at 300°C for alloys different Mo content after precipitation treatment	67
Fig. 4.16 Evolution of (a) electrical conductivity at 375°C; (b) microhardness at 375°C; (c) electrical conductivity at 425°C; (b) microhardness 425°C for Base 3004 and M30 alloys during precipitation treatment	70
Fig. 4.17 Evolution of electrical conductivity for base 3004 and M30 alloys during precipitation treatment at different temperatures (a) 475°C, (b) 500°C, (c) 525°C, (d) 550°C, (e) 600°C	73
Fig. 4.18 Evolution of microhardness for base 3004 and M30 alloys during precipitation treatment at different temperatures (a) 475°C, (b) 500°C, (c) 525°C, (d) 550°C, (e) 600°C.....	74
Fig. 4.19 Microhardness for base 3004 and M30 alloys after precipitation treatment for 24 hours at different temperature.....	76
Fig. 4.20 Yield strength at 300°C for base 3004 and M30 alloys after precipitation treatment for 24 hours at different temperature	78
Fig. 4.21 (a)Electrical conductivity and (b) Microhardness evolution during the second step precipitation treatment at 500°C after the first precipitation treatment at 375°C	

for 48 hours	79
Fig. 4.22 Evolution of YS at 300°C during the second step precipitation treatment at 500°C after precipitation treatment at 375°C for 48 hours	80
Fig. 4.23 Compressive creep curves at 300°C	81
Fig. 4.24 Microhardness evolution during long thermal holding at different temperature (a) 350°C; (b) 400°C.....	83
Fig. 4.25 Evolution of YS at 300°C during long thermal holding at different temperature (a) 350°C; (b) 400°C.....	83
Fig. 4.26 Evolution of YS during long thermal holding at different temperature holding and tested at (a) 350°C; (b) 400°C.....	84
Fig. 4.27 Evolution of YS at different temperature after peak precipitation treatment(375°C/48h)	85
Fig. 4.28 The microhardness for different holding times during the first step precipitation treatment at (a) 175°C, (b) 250°C and (c) 330°C	89
Fig. 4.29 YS at 300°C for different preheating treatment.....	90
Fig. 4.30 Long-term thermal holding results (a) at 350°C (b) at 400°C.....	91
Fig. 4.31 Compressive creep curves at 300°C for (a)base 3004 alloy, (b) M30 alloy with preheating at 250°C	91

1 Introduction

1.1 Definition of problem

In past decades, wrought aluminum alloys are widely used in many industrial fields because of the high strength-to-weight ratio, great corrosion resistance and relatively low cost. Currently, the development of automobile and aerospace industries promote the demand of aluminum alloys that possess competitive properties at elevated temperatures(250°C-300°C). For precipitation strengthening wrought aluminum alloys, such as 2xxx, 6xxx and 7xxx alloys, they can have high strengths at temperatures up to 100°C due to the fine and uniformly distributed precipitates formed during the heat-treatment[2]. However the mechanical properties of these alloys decline rapidly due to the coarsening of the precipitates (overaging) at elevated temperature[3, 4]. Therefore, developing low cost aluminum alloys that function well at elevated temperature is particularly attractive for industries.

Al-Mn 3xxx alloys are one of the widely used commercial aluminum alloys, which have been used in many industrial sectors, such as architecture and packaging industry. 3xxx alloys are generally strengthened by work hardening and classified as non-heat treatable alloys [5, 6]. However, recent research found out that 3xxx alloys can form a considerable amount of dispersoids during heat treatment, which can contribute to the strength at elevated temperature[7-11], providing the possibility for 3xxx alloys for the elevated-temperature

applications

As the principal alloying element in 3xxx alloy, Mn can dissolve and form supersaturated solid solution in aluminum matrix after solidification. During the heat treatment, the dispersoids form from the decomposition of the Mn solid solution. Many research have studied the precipitation behavior of the dispersoids in 3xxx alloys[5, 9, 10, 12-15]. The type of the dispersoids varies with alloy composition and heat treatment. $Al_6(MnFe)$ phase tends to precipitate with low Si content and high temperature, while $\alpha-Al(MnFe)Si$ prefers to precipitate with high Si level and low temperature[16-18].

The $\alpha-Al(MnFe)Si$ dispersoids is reported to have strong influence on the recovery and recrystallization of aluminum alloy [19, 20]. It is also reported to have a considerable effect on mechanical properties in 3xxx alloys[10, 17, 21]. The work of Liu et al.[11] shows that the dispersion strengthening effect provide by $\alpha-Al(MnFe)Si$ dispersoids can be achieved by the precipitation treatment, and have significant improvement on the YS and creep resistance at 300°C. Meanwhile, the $\alpha-Al(MnFe)Si$ dispersoids are approved to be thermally stable at 300°C.

However, recent research shows that the precipitation of dispersoids become less and coarse after homogenization, which is a necessary industrial high temperature treatment (450°C-600°C). Meanwhile, the diffusion of Mn to the primary intermetallic $Al_6(MnFe)$ as well as the increasing of dispersoid free zone(DFZ) at high temperature lead to the decreased

properties [13, 22]. To solve this problem, possible elements, which have low diffusion rate and to form potential dispersoids under higher temperature can be added, and Mo is one of the candidates[23, 24].

As a transitional element, Mo has relative low diffusivity, which makes Mo become a potential alloying addition to aluminum alloys that may provide hardening effects at elevated temperature. Recent research shows that Mo addition in Al-Si-Cu-Mg and Al-Si-Cu-Mg-Mn alloys can have significantly contribute to its elevated temperature properties[23, 24]. The Mo addition in these alloys provides more uniformly distributed and thermal stabilized dispersoids. However, limited work has been performed on the behavior of dispersoids in Al-Mn-Mg 3004 alloys with Mo as well as their influence on properties, especially at elevated temperature.

1.2 Objective

The objective of this project is to investigate the influence of Mo additions on the dispersoid precipitation behavior and properties of AA3004 alloy. The research plan is arranged into different parts as below:

1. Investigating the characters of Mo in AA3004 alloy.

Modified AA3004 ingots with various levels of Mo addition are designed to study the characters of Mo, such as the solubility and formation of primary Mo-rich intermetallic particles, to fully understand the state of Mo in AA3004 alloys.

2. Studying the influence of Mo on the dispersoids precipitation behavior.

A series of precipitation treatment at different temperature and holding time will be designed to study the influence of Mo addition on the precipitation behavior of dispersoids in AA3004 alloy.

3. Exploring the effects of dispersoids (with or without Mo addition) on the properties of AA3004 alloy.

Microhardness, electrical conductivity and mechanical properties as well as the creep test and thermal stability of alloy at elevated temperature will be applied after precipitation treatment to explore the effect of Mo addition on the properties.

2 Literature review

2.1 Elevated temperature applications of aluminum alloys

In past three decades, aluminum alloys have been developing for the application at the elevated temperature range from 250 to 350°C. Precipitation hardening aluminum alloys can't keep their high strength at elevated temperature due to the coarsening of the precipitates (overaging). Therefore, developing a low-cost, thermal stable aluminum alloys for elevated temperature applications is always attractive in industries, such as automobile and aerospace industries.

Dispersion strengthening is reported to be a significant mechanism to improve the elevated temperature mechanical properties of aluminum alloys[8, 23, 25, 26]. Therefore, potential alloys that can form a large amount of thermal stable dispersoids during heat treatment are always the candidate for elevated temperature applications. To reach this goal, the alloying elements acting as dispersoid former should have moderate solubility in liquid aluminum and low solubility as well as low diffusion rate in solid aluminum. With relative high solubility in liquid aluminum, they can be added with a large amount and form supersaturated solid solution after rapid solidification. During heat treatment, with the decomposition of the solid solution, they can precipitate out a high volume fraction of dispersoid phase if these elements also have low solubility in solid aluminum. If these

dispersoids have good thermal stability, their presence is desirable and will contribute to the mechanical properties by blocking the movement of dislocations and decrease the spacing between particles by increased secondary phase volume fraction.

Many aluminum alloys, such as Al-Fe-Ce, Al-Fe-V-Si, Al-Fe-Mo(-V), Al-Cr-Zr(-Mn), Al-Ti-Fe, etc. have been successfully developed for elevated temperature applications by the rapidly solidified powder metallurgy (RS P/M) process. All these alloys are based on Al-TM (TM=transition metal) type systems, and the elevated temperature strength of these alloys derives from the presence of a large (15 to 35%) volume fraction of fine and stable intermetallic dispersoids[27]. These alloys have been received great attention because they possess much better high temperature strengths compared to conventional aluminum alloys, and also exhibit the potential to replace titanium alloys used in aerospace in the temperature range from 250 to 350°C.

Table. 2.1 shows the tensile properties of Al-Fe-Ge and Al-Fe-V-Si alloys under different temperatures, from 298K (25°C) to 573K (300°C). It can be found that both alloys possess a yield strength over 200MPa under 300°C, and the results for other systems like Al-Fe-Mo(-V), Al-Cr-Zr(-Mn), Al-Ti-Fe are quite similar, indicating that all these Al-TM alloys have good elevated temperature strength[26-28]. However, all these alloys are produced by the rapidly solidified powder metallurgy (RS P/M) process and the high cost limited their application in commercial aluminum alloys.

Table 2.1 Tensile properties of Al-Fe-Ce and Al-Fe-V-Si alloys[27]

Alloy	Test temperature (K)	0.2%	Tensile strength (MPa)	Total	Uniform
		Yield strength (MPa)		plastic	plastic
				elongation	elongation
				(%)	(%)
Al-Fe-Ce	298	486	560	2.1	2.1
	473	276	292	6.2	1.6
	573	209	209	4.4	0
Al-Fe-V-Si	298	358	420	9.2	2.3
	473	274	294	4.8	1.5
	573	208	208	4.2	0

As for the wrought aluminum alloys application at elevated temperature, Al-Mn 3xxx alloys show their potential to be a great candidate. Comparing with other wrought aluminum alloys, relatively higher elevated-temperature properties can be achieved in Al-Mn3xxx alloys, in which α -Al(Mn,Fe)Si dispersoids are formed under relative higher temperature and they are quite stable at elevated temperature[9, 11]

2.2 Al-Mn 3xxx alloys

Wrought 3xxx aluminum alloys, are widely used in the production of the seamless body in

two-piece all-aluminum cans, chemical handling and storage equipment, sheet metal work, builders' hardware, incandescent and fluorescent lamp bases and similar applications requiring good formability and higher strength due to the relatively low cost, good workability, and excellent corrosion resistance. Recent researches reveal that both dispersion strengthening and solution strengthening can be applied to Al-Mn 3xxx alloys to improve the properties. Dispersion strengthening is treated as the most important strengthening mechanism at elevated temperature because of the relatively stable dispersoid particles, which are formed after precipitation treatment. These dispersoids are proved to be thermal stable and can make significant improvement on alloy's elevated temperature properties[7-9, 11].

2.2.1 The effect of alloying elements

The chemical composition of traditional commercial 3004 alloys is as shown in Table 2.2 .

Table 2.2 Composition limits of 3004 alloys[1]

	Mn	Si	Fe	Cu	Zn	Mg	Al
Wt%	1.0-1.5	0.30	0.70	0.25	0.25	0.8-1.3	bal

Mn:

The binary phase diagram of Al-Mn is shown in Fig. 2.1. It can be found that as much as 1.82wt% can be soluble in Al. However, Mn content in commercial Al-Mn alloy is often less than 1.25wt. % (all the compositions are in wt.% in present work unless indicated otherwise) [2]. As the major alloying element in 3004 alloy, Mn influences the material properties in different ways. First, Mn makes the alloys ductile, resulting in good formability, also good corrosion resistance. Second, the amount and size of Mn-containing intermetallic particles affect the grain structure during solidification and heat-treatment[2]. During the solidification, most of the Mn atoms can be solid-dissolved in the aluminum matrix, which forms a supersaturated solid solution that can contribute to the strengthening of the material by solid solution hardening. The remaining Mn is present as $Al_6(Mn,Fe)$ constituent particles. During precipitation treatment, $\alpha-Al(Mn,Fe)Si$ dispersoids precipitate from the supersaturated matrix. Higher supersolid level of Mn will favor the precipitation of $\alpha-Al(Mn,Fe)Si$ dispersoids with

high density and volume fraction.[10].

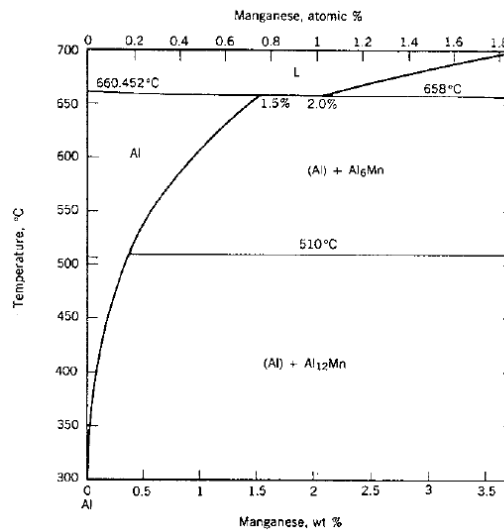


Fig. 2.1 Al-Mn phase diagram[2]

Si:

Si has a major influence on the constituent particles transformation from Al₆(Mn,Fe) to α-Al(Mn,Fe)Si as it is the only element required for transformation [29]. Raising the level of Si in the alloys raises the proportion of α-Al(Mn,Fe)Si constituent particles and the transformation rate from Al₆(Mn, Fe) to α-Al(Mn,Fe)Si. Si also speed up the precipitation of dispersoids α-Al(Mn,Fe)Si by reducing the solubility of Mn in Al matrix. In alloys that contain high Si content, α-Al(Mn,Fe)Si dispersoids are a stable phase and less Al₆(Mn,Fe) dispersoids will precipitate. However, α-Al(Mn,Fe)Si dispersoids can precipitate at relatively low temperatures but dissolve at high temperatures and Al₆(Mn,Fe) dispersoids will precipitate as a stable phase in alloys that with low Si content[9].

Mg:

When Mg is added to aluminum alloys with Si, Mg_2Si particles precipitate from matrix. With aging treatment, large amount of nano-scale Mg_2Si particles can be obtained. As for 3004 alloys, the amount of Mg_2Si phase is too small to cause an appreciable precipitation hardening effect because that most of the Si is combined as the $\alpha-Al(Mn,Fe)Si$ phase during the homogenization and hot rolling process of the alloy. Besides, the precipitation temperature for $\alpha-Al(Mn,Fe)Si$ dispersoids is too high for Mg_2Si . At the range of 300°C to 500°C, Mg_2Si will coarsen fast or dissolve in the matrix. However, Mg has a very high solid solubility in aluminum (up to 14.9% at 450°C and still 1.7% at room temperature(Fig. 2.2)). Therefore solid solution hardening is easily achieved by adding Mg, which makes the strength of 3004 alloys higher than 3003. However, high content of Mg will decrease the workability[1, 2].

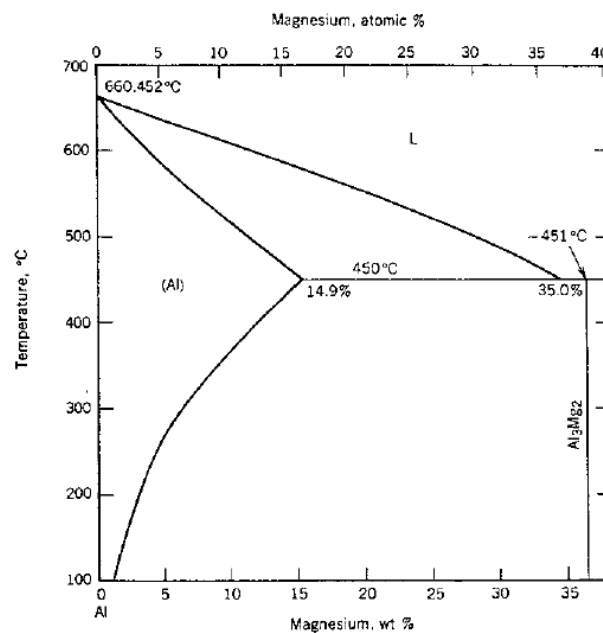


Fig. 2.2 Al-Mg phase diagram[2]

Fe:

Fe favors the formation of $Al_6(Mn, Fe)$ and $\alpha-Al(Mn,Fe)Si$ intermetallic particles. In these two phases, Fe and Mn can substitute each other freely. Also, Fe greatly decreases the solubility of Mn in solid solution and accelerates the formation rate of intermetallic particles. With high Mn/Fe ratio, $\alpha-Al(Mn,Fe)Si$ phase has a simple cubic crystal structural, but the phase may change to a body centered cubic structure with increasing Fe content [5].

2.2.2 The evolution of constituent particles during heat treatment

The primary particles in Al-Mn-Si 3xxx alloys after solidification are eutectic constituent particles, including $\text{Al}_6(\text{Mn, Fe})$ and $\alpha\text{-Al}(\text{Mn,Fe})\text{Si}$ that distributed in the interdendritic regions. It has been found that the composition of these primary particles can change and some of the $\text{Al}_6(\text{Mn, Fe})$ particles will transfer into $\alpha\text{-Al}(\text{Mn,Fe})\text{Si}$ during heat-treatment.

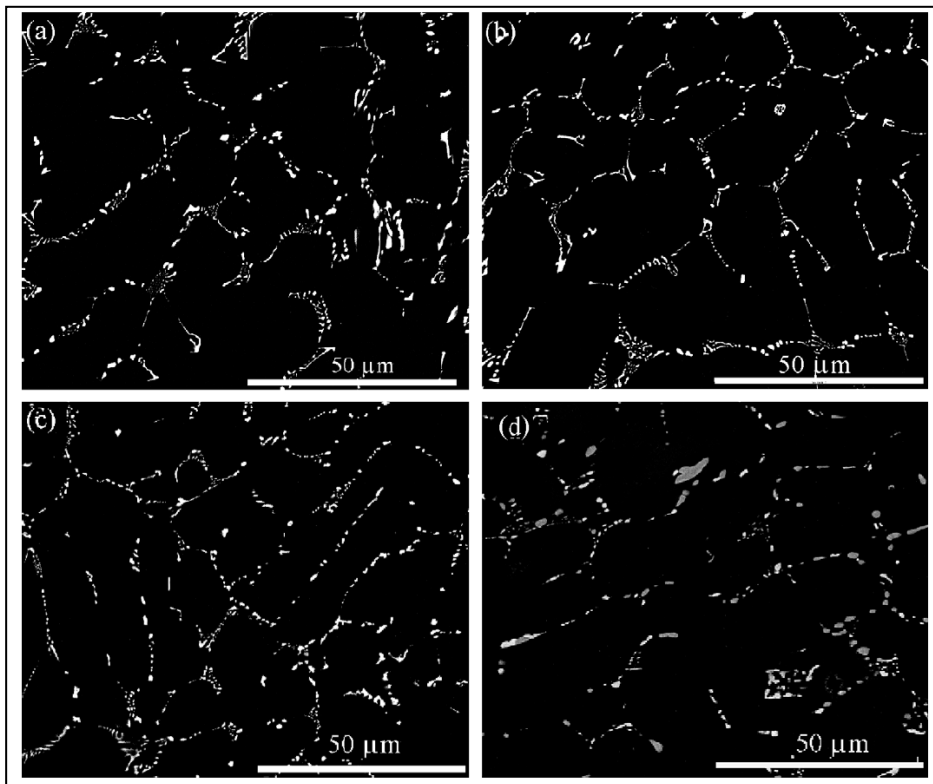


Fig. 2.3 Back scatter electron SEM images of primary particles (a) in the as-cast state and quenched from (b) 400°C, (c) 560°C and (d) 630°C during heating[30]

The microstructure of 3xxx alloys is shown in Fig. 2.3a. It can be found that large amounts of rod like or plate like intermetallic particles are distributed in the interdendritic regions and grain boundaries. Most of the intermetallic particles have been determined to be $\text{Al}_6(\text{Mn,Fe})$

and only a small fraction of primary particles are identified as α -Al(Mn,Fe)Si. When annealing temperature goes up, the number density of intermetallic particles increases. The eutectic networks and long rod like intermetallic particles are broken up into small particles during heating from 400 °C to 560 °C (Fig. 2.3a-c). At this stage, the size evolution is caused predominantly by spheroidization. However, if the temperature is high enough, the number density will drop sharply and the diameter increases, which indicates that coarsening is the main mechanism to control the evolution of primary, as is shown in Fig. 2.3d.

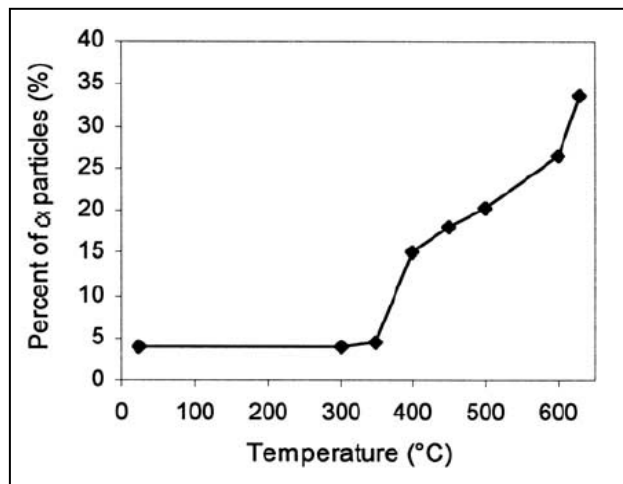


Fig. 2.4 Fraction of α -Al(Mn,Fe)Si in total amount of primary particles[30]

Fig. 2.4 shows the evolution of particles during the annealing process in 3003 alloys[30]. It can be found that the fraction of α -Al(Mn,Fe)Si increases sharply with temperature, resulted by the transformation from $Al_6(Mn,Fe)$ into α -Al(Mn,Fe)Si. The transformation process from $Al_6(Mn,Fe)$ to α -Al(Mn,Fe)Si is identified as a eutectoid process in which the $Al_6(Mn, Fe)$ phase decomposes to a mixture of α -Al(Mn,Fe)Si and aluminum solid solution. The transformation occurs at about 400°C, and the fraction of α -Al(Mn,Fe)Si in total amount of

primary particles increase with temperature.

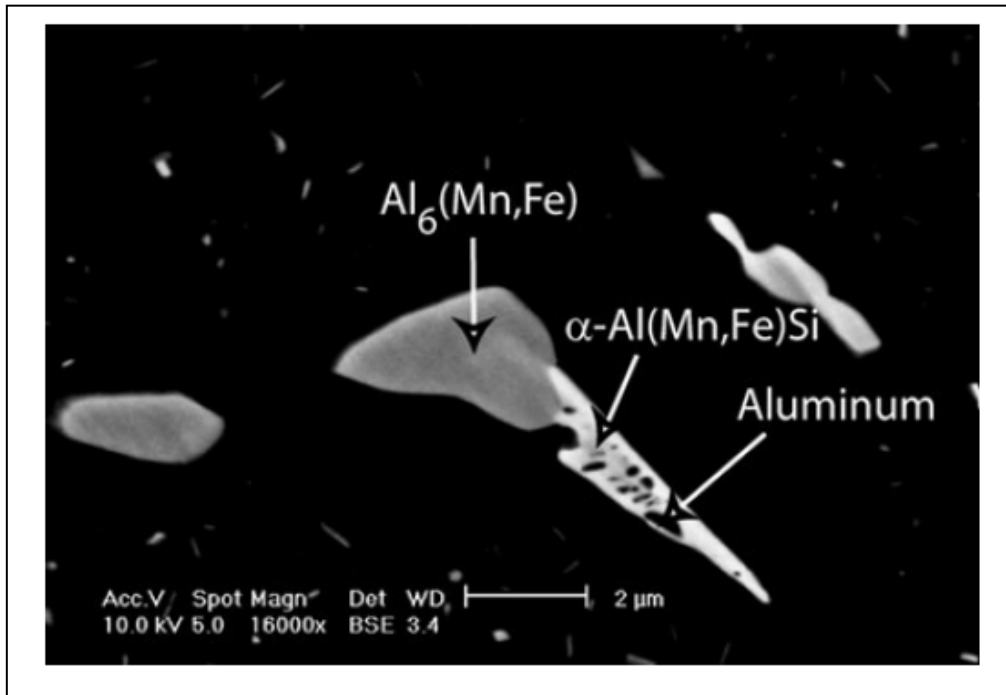


Fig. 2.5 Back scatter SEM image revealing the eutectoid transformation of the primary particles $Al_6(Mn, Fe)$ into $\alpha-Al(Mn,Fe)Si$ [31].

Fig. 2.5 shows the co-exist $\alpha-Al(Mn,Fe)Si$ and $Al_6(Mn,Fe)$ particles during the transformation in 3xxx alloy[31]. It can be seen that the dark $Al_6(Mn,Fe)$ is transferring to $\alpha-Al(Mn,Fe)Si$. The decomposition preserves the local volume and content of Fe and Mn, which diffuse slowly[32], but requires intake of Si. The Si appears to diffuse from the matrix, and the degree of the $Al_6(Mn,Fe)$ to $\alpha-Al(Mn,Fe)Si$ transformation appears to be thermodynamically limited by the supply of Si.

2.2.3 Dispersoid particles and their evolution in Al-Mn-Si 3xxx alloys

In commercial 3xxx alloys, previous researches have been done to study the precipitation behavior of dispersoids[5, 9, 10]. There are two principal types of dispersoids that can form in 3xxx alloys containing Mn, Fe and a certain level of Si content. They are orthorhombic type $\text{Al}_6(\text{Mn,Fe})$ dispersoids and cubic $\alpha\text{-Al}(\text{Mn,Fe})\text{Si}$ dispersoids. The proportion between these two dispersoids is influenced by the chemical composition, especially by the Si content. In the alloys with high Si content, $\alpha\text{-Al}(\text{Mn,Fe})\text{Si}$ dispersoids will precipitate as a stable phase and there are no $\text{Al}_6(\text{Mn, Fe})$ dispersoids. In the alloys with low Si content, $\alpha\text{-Al}(\text{Mn,Fe})\text{Si}$ dispersoids will precipitate at low temperature but dissolve at high temperature. Instead, $\text{Al}_6(\text{Mn,Fe})$ dispersoids will precipitate as the stable phase[10]. It has been found that $\text{Al}_6(\text{Mn,Fe})$ dispersoid particles tend to precipitate during low-temperature homogenization, while $\alpha\text{-Al}(\text{Mn,Fe})\text{Si}$ dispersoid particles tend to precipitate at high temperature[30]. Increasing the temperature or extending the duration of the homogenization treatment causes some of the $\text{Al}_6(\text{Mn,Fe})$ particles to redissolve and transform into $\alpha\text{-Al}(\text{Mn,Fe})\text{Si}$ dispersoid particles. The $\alpha\text{-Al}(\text{Mn,Fe})\text{Si}$ dispersoids precipitate in a lot of commercial alloys containing Si and Fe/Mn, and because of its positive effects on the alloy properties, $\alpha\text{-Al}(\text{Mn,Fe})\text{Si}$ dispersoids is proved to be the most important dispersoids in 3xxx alloys.

The $\alpha\text{-Al}(\text{Mn,Fe})\text{Si}$ dispersoids in 3xxx alloys have influence on retarding the recovery

and recrystallization behavior, which has been well investigated in last several decades[33-35]. As those dispersoids have relatively large size and low number density, they are usually considered to have no hardening effect in 3xxx alloys. However, recent researches revealed that a reasonable amount of dispersoids can precipitate during heat treatment and have a significant strengthening effect in 3xxx alloys[9-11].

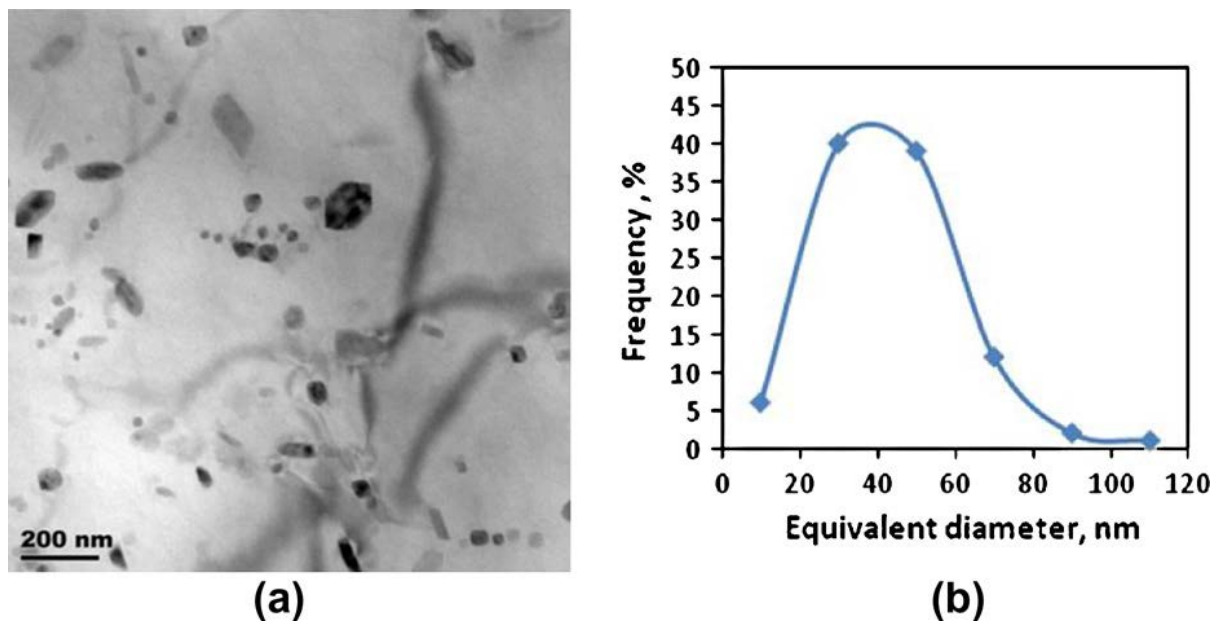


Fig. 2.6 TEM image (a) and size distribution (b) of dispersoids after 24h annealing at 375°C.[9]

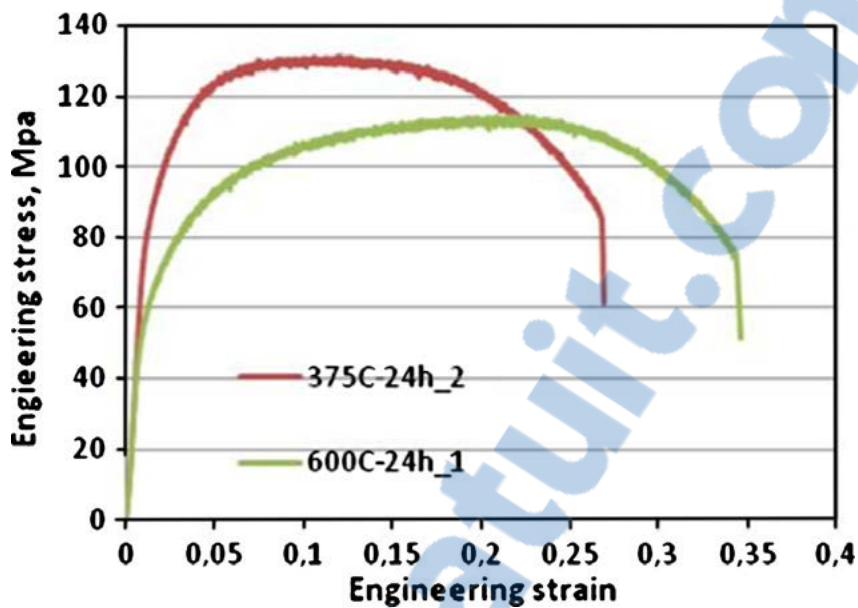


Fig. 2.7 The stress-strain curve of the annealed specimen and the homogenized specimen. [9]

Fig. 2.6 shows the morphology and size distribution of dispersoids that formed in the 3xxx alloy after 24h of annealing at 375°C[9]. It can be found that there is a large number of fine dispersoid formed in Al matrix. Fig. 2.7 shows that there is a significant increase in yield strength of the alloy after annealing at 375°C after 24h than the as-homogenized condition, which is attributed to the dispersion strengthening[9]. The work of Muggerud et al.[10] shows that 3xxx alloy that contains high amount of Mn and Si content can achieve pronounced dispersion hardening effect after treated at 375°C for more than 12 hours. Both microhardness, yield strength and tensile strength have been much improved. The hardening effect from dispersoids can explained by the Orowan bowing mechanism of dispersoids. The study of Liu et al.[11] shows that a significant dispersion strengthening can be achieved in

AA3004 alloy by precipitation treatment at 375°C for 48 hours. The large volume fraction of the fine and uniformly distributed dispersoids can improve the yield strength at elevated temperature, as shown in Fig. 2.8. Meanwhile, the dispersoids also appeared to be thermally stable at 300°C. As shown in Fig. 2.9, the EC, hardness and yield strength of the alloy were stable during holding at 300°C for 1000 hours.

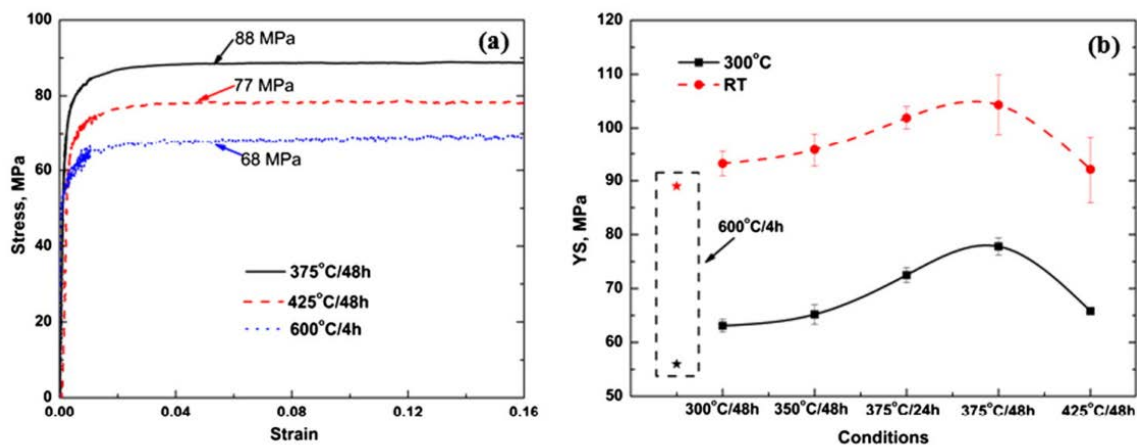


Fig. 2.8 True stress-strain curve (a) and YS at both RT and 300°C and different treatment conditions (b)

for AA3004 alloy[11]

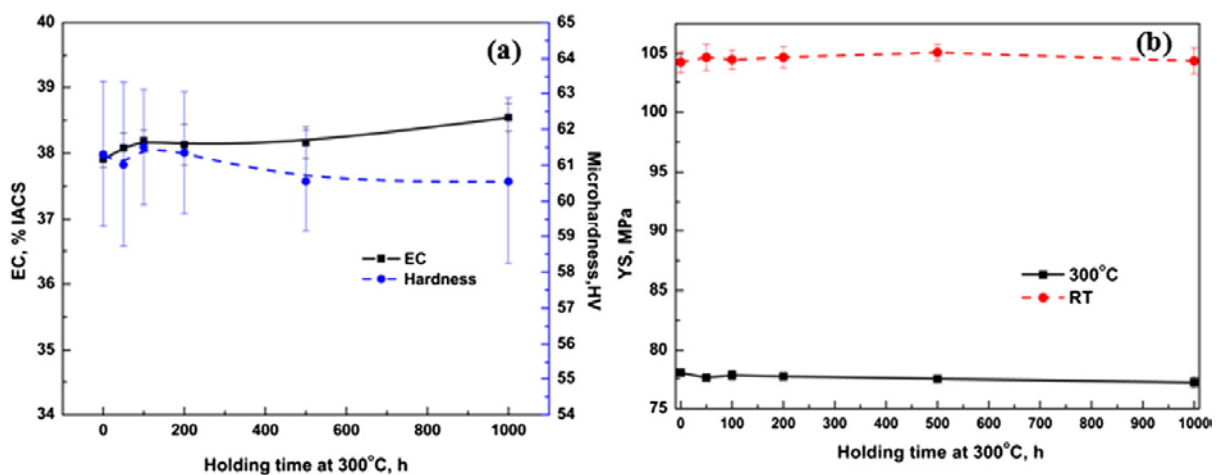


Fig. 2.9 Evolution of EC and hardness (a) and YS (b) during a long thermal holding[11]

The precipitation behavior of the α -Al(Mn,Fe)Si dispersoids is deeply related with the temperature. Fig. 2.10 shows the electrical conductivity evolution of 3003 alloy during heat treatment. The EC of 3xxx alloy can be used to estimate the concentration of Mn in solid solution and give a indication of the decomposition reaction of the solid solution during heat treatment[5]. This result shows that during heating of 3003 alloy, the supersaturated solid solution starts to decomposition at 300°C and keep decomposing with increasing temperature. The decrease of EC after 530°C is caused by the increase of solubility of Mn, which make the dispersoids dissolve into the matrix.

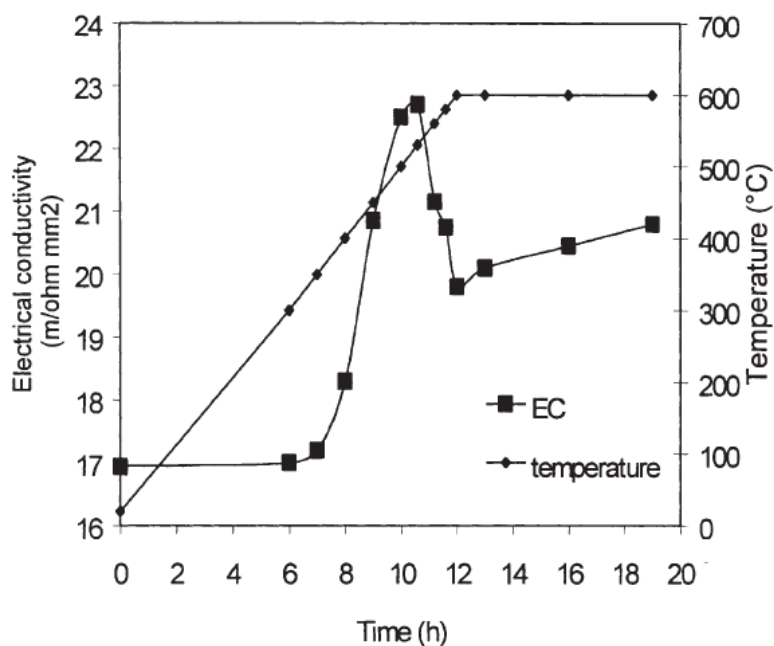


Fig. 2.10 Electrical conductivity evolution of 3003 alloy during heat treatment.[5]

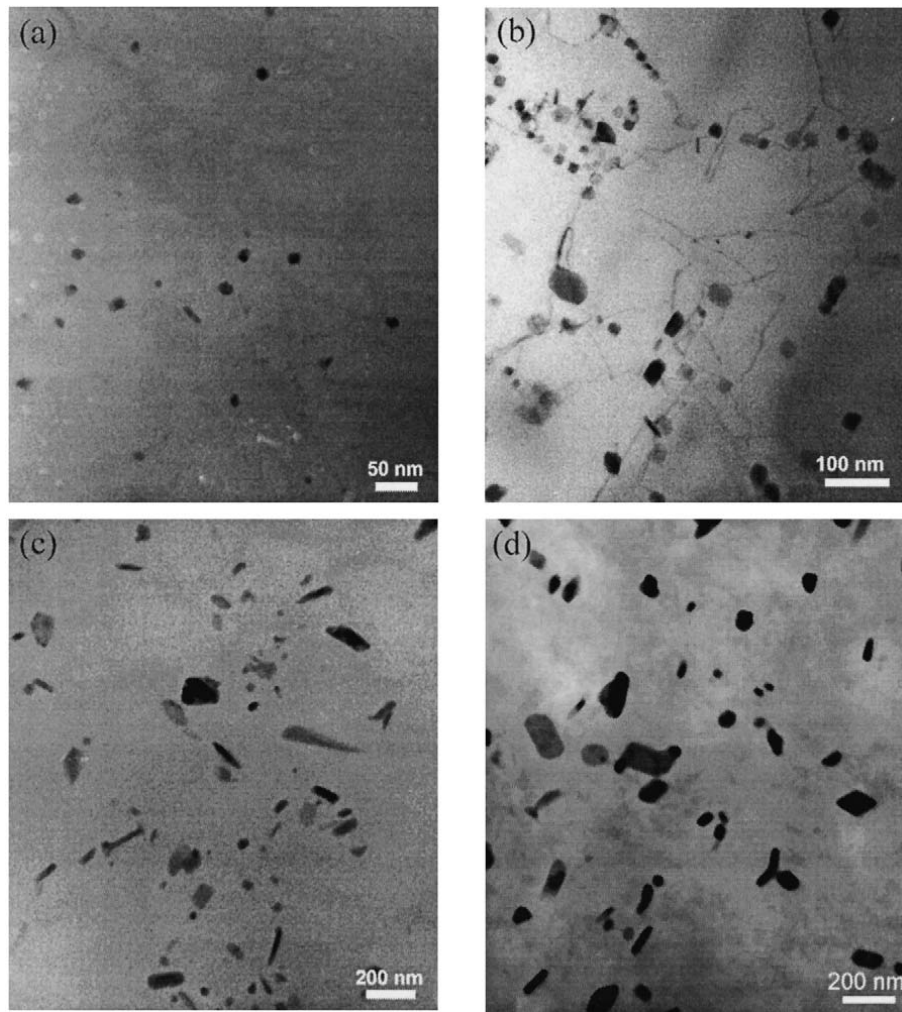


Fig. 2.11 TEM morphology of dispersoids precipitated during heating in 3003 alloy. (a) 350°C (b) 400°C
(c) 500°C (d) 580°C[5]

The precipitation of dispersoids occurs with the decomposing of supersaturated solid solution. Fig. 2.11 shows the morphology of dispersoid precipitated during heating. When the temperature reached 300°C, very fine dispersoids can be found in the aluminum matrix as soon as the decomposition begins. With increasing temperature, the dispersoids become more and larger and with the morphology developed into plate-like and rod-like shapes.

Fig. 2.12 shows the number density and size evolution of dispersoids during heating[5].

The number density of the dispersoids increases with increasing temperature and reaches the maximum point at around 400°C. Meanwhile, the size of the dispersoids increases with increasing temperature. In general, dispersoids with fine size and high volume fraction can have great dispersion strengthening effect in aluminum alloys. Based on the results of recent work[5], precipitation treatment at 375°C for 48 hours is the most effective heat treatment procedure to get desirable dispersoids in 3xxx alloys.

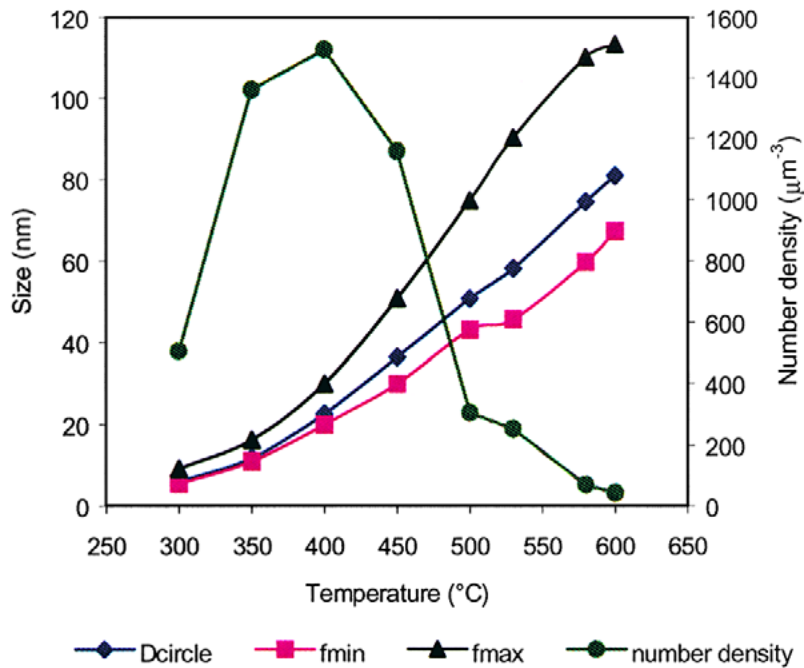


Fig. 2.12 Size and number density evolution of dispersoids during heating in 3003 alloy.[5]

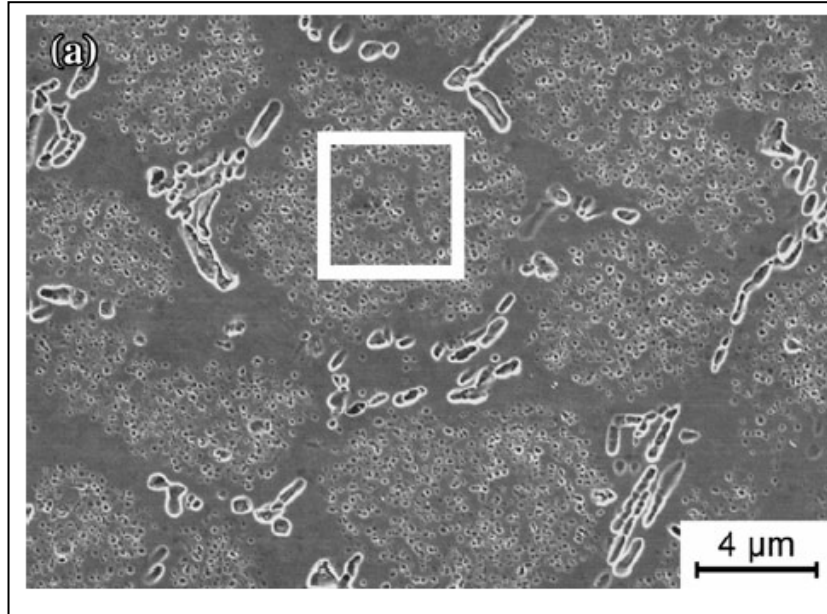


Fig. 2.13 SEM images which show the location of dispersoids[31]

Fig. 2.13 shows the distribution of the dispersoids in which alloy[31]. Most of the dispersoids distribute in dendrite arms, except for a large fraction of dispersoid free zones (DFZ) on the grain boundaries and interdendritic areas. All the DFZ areas locate in the Mn depleted areas formed during solidification[12]. The diffusion of Mn in the matrix is the key factor of the precipitation and size evolution of dispersoids, as well as the formation of DFZ. Dispersoids particles can and only can nucleate in the Al matrix where has high level of Mn content. Thus most of the dispersoids nucleate in dendrite arms instead of the Mn depleted areas at interdendritic region around constituent particles. With increasing temperature, more and more Mn precipitate from the supersaturated solid solution into the dispersoids in dendrite arms, leading to the growth of these dispersoids. With the low diffusion rate of Mn in Al matrix at low temperature, long distance diffusion of Mn is almost impossible, which

means the precipitation of dispersoids is controlled by nucleation and growth at low temperature. With continuously increasing temperature, the number density of dispersoids reaches the maximum amount, and with the increasing diffusion rate of Mn, coarsening of the dispersoids occurs and became dominantly. Dispersoids will have decreased number density and increased size with further increasing temperature. With temperature higher than 530°C, some of the dispersoids will dissolve because of the increased solubility of Mn. Meanwhile, the dispersoids surrounding the primary constituent particles will also dissolve due to the coarsening of constituent particles, which means the area of DFZ will also increase.

Beside the Mn depleted areas at interdendritic region around constituent particles, there is another location of DFZ in AA3004 alloy. Fig. 2.14 showed the formation of DFZ in AA3004 alloy treated at 425°C for 48 hours. The region B in Fig. 2.14a is located in the intradendritic region. The formation of the DFZ in intradendritic regions is caused by the microsegregation of Mn content after solidification. Since Mn has a solid-liquid partition coefficient, $k_0 = C_s/C_L < 1$, which makes Mn segregates towards the interdendritic region. Therefore, the concentration of Mn in the intradendritic is low after solidification, making the dispersoid precipitation difficult[11].

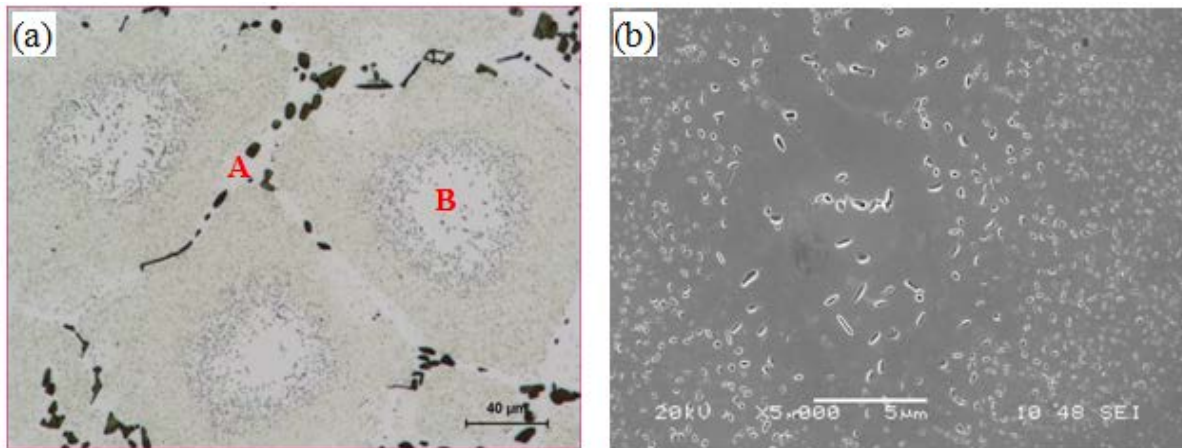


Fig. 2.14 Formation of DFZ in AA3004 alloy treated at 425°C for 48h: (a)OM and (b)SEM, an enlargement of (a).[11]

The existence of DFZ will have negative influence on the mechanical properties of the alloy and also can decrease the alloy's real dispersoids quantity and number density, since the quantity and number density are all normally observed under TEM within the dispersoids containing region. In order to get the optimal strengthening effect via dispersoid particles, the temperature and holding time for precipitation treatment should be carefully controlled to reduce the area of DFZ.

2.3 Effects of Mo addition on properties

Effective dispersoids to improve elevated temperature properties need to be thermally stable and have high volume fraction as well as uniform distribution in Al matrix. The thermal stability of the dispersoids depends on the low solid solubility and diffusivity of the constituent solute atoms in the Al matrix. The development of Al alloys for elevated temperature applications can follow two basic routes: (i) Slowing down the coarsening kinetics of age hardening precipitates by adding trace additions such as Ce and Ge.[27] (ii) Getting thermally stable precipitates or dispersoids that can retain their effectiveness under elevated temperature. Hence, the transition and rare earth elements are potential candidates as dispersoid formers.

A series of these elements have been already studied as dispersoids formers in wrought Al alloys. Zirconium (Zr) forms coherent Al_3M type dispersoids in Al alloys[36], which has the great ability of resistance against recrystallization but very low strengthening effect[37]. Scandium (Sc) also forms coherent Al_3M type dispersoids but its use in commercial Al alloys is limited because of its high cost[28]. Chromium (Cr) forms face centered cubic (FCC) $\alpha-AlCrSi$ dispersoids in wrought and casting Al alloys but the strengthening effect is negligible[26].

As a dispersoids former, Molybdenum (Mo) has been used in rapidly solidified (RS) powder metallurgy Al alloys for elevated temperature applications[5]. Because of its low diffusivity in Al ($3.2 \times 10^{-20} m^2 s^{-1}$ at $300^\circ C$)[24] and the limited solid solubility in Al (~ 0.25

wt. % at 660°C), which also decreases rapidly with decreasing temperature (Fig. 2.15), makes it an interesting candidate as dispersoids former for Al alloys.

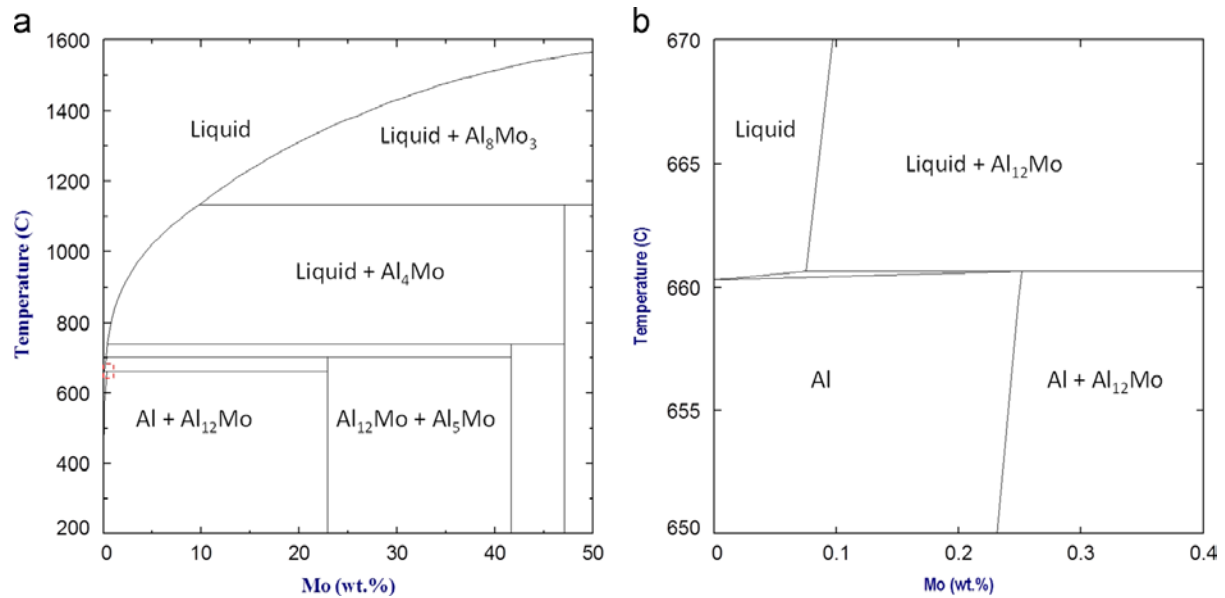


Fig. 2.15 (a)Al–Mo binary phase diagram and (b) enlarged view of the Al-rich corner (calculated using FactSage software).[23]

However, the current study for Mo in Al wrought alloys has not got much attention because that Mo-containing dispersoids phase does not form under the conditions of conventional aging temperature. Reliable study and data for phase selection and precipitation of Mo containing alloys are scarce but, it has the potential to form a large amount of metallurgically stable dispersoids in Al wrought alloys. Fig. 2.16 shows the Al–(Fe,Mo)–Si dispersoids forms after solution treatment in Al-Si cast alloys[23]. It reveals that Mo can form a considerable amount of fine and thermal stable dispersoids in Al-Si cast alloy, even with very low content(0.3wt%). These dispersoid have positive effects on the elevated temperature

properties. Fig. 2.17 shows the tensile properties of the Al-Si cast alloys at 300°C. It can be shown that both the YS and UTS has significant improved by Mo addition.

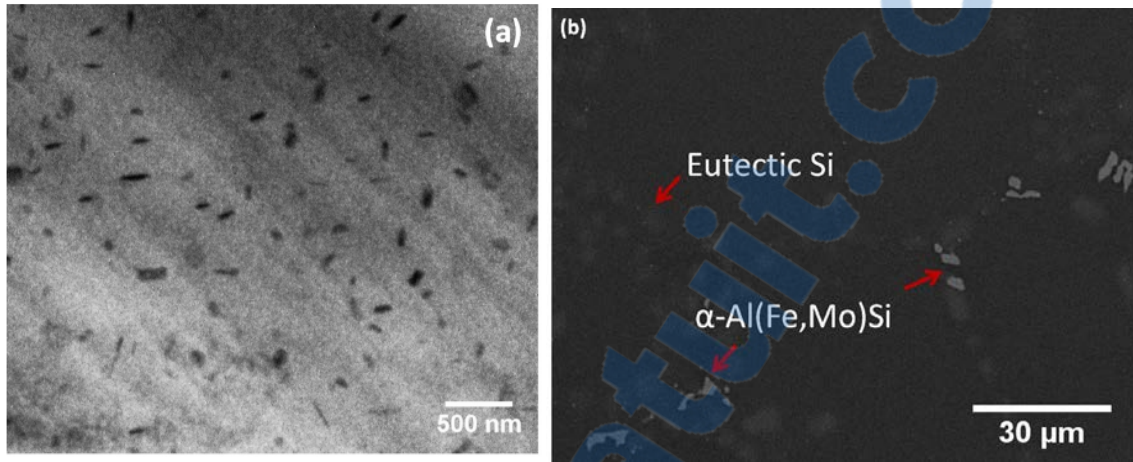


Fig. 2.16 (a) Bright field TEM micrograph showing the Al-(Fe,Mo)-Si dispersoids in the intradendritic regions of the Mo-containing Al-Si cast alloy formed after 10h of solution treatment at 540°C. (b) Back scattered SEM micrographs showing the solution treated (4h at 500°C and 10h at 540°C) microstructures of the Mo-containing Al-Si cast alloy[23].

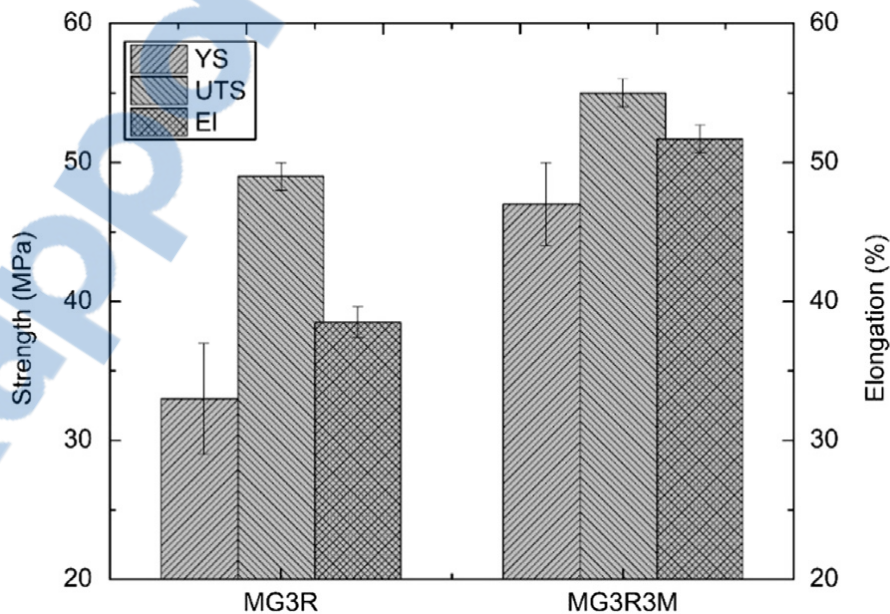


Fig. 2.17 Tensile properties of the alloys at 300°C. Solution treated at 540°C for 10h, aged at 200°C. For 5h

and soaked at 300°C for 100h[23].(MG3R3M alloy is made by adding 0.3% Mo addition into MG3R alloy)

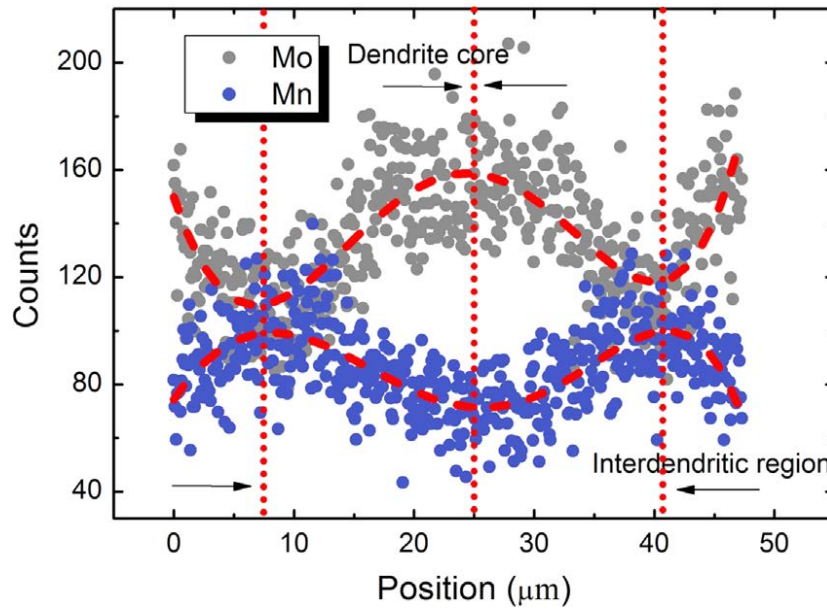


Fig. 2.18 EDS elemental line scanning across a dendrite cell showing the concentration gradients of Mo and Mn (microsegregation) in the as-cast Al-7Si-0.5Cu-0.3Mg-0.1Fe-0.3Mo-1.5Mn alloy.[24]

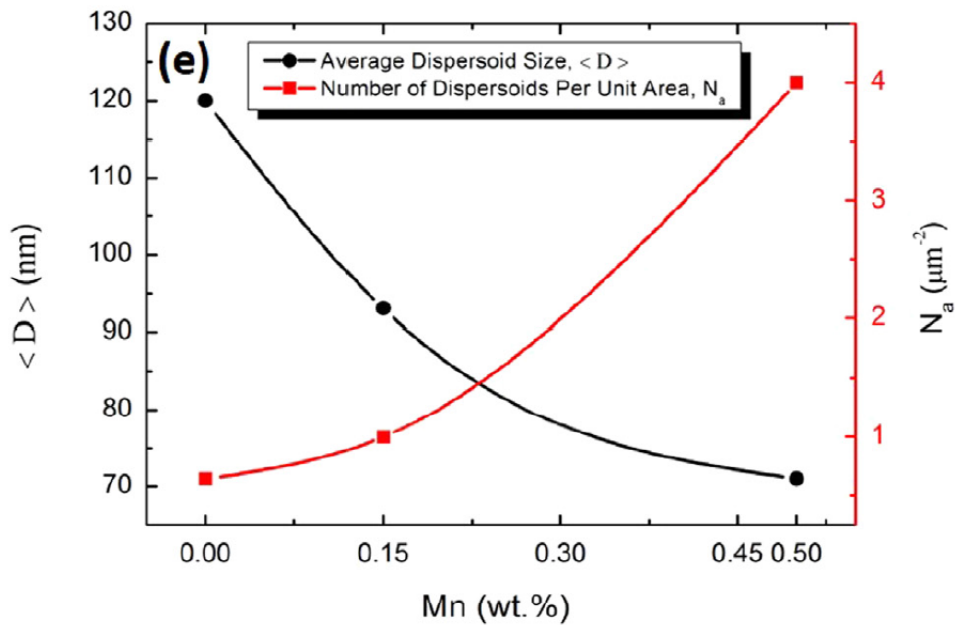


Fig. 2.19 Average dispersoid size and the number of dispersoid per unit area of the α - Al(Fe, Mn, Mo)Si in Al-7Si-0.5Cu-0.3Mg-0.1Fe-0.3Mo-1.5Mn alloy.[24]

Moreover, Mo has a solid-liquid partition coefficient, $k_0 = C_s/C_L > 1$ as a peritectic element, which makes Mo segregates towards the intradendritic regions after solidification. Meanwhile, Mn has a $k_0 = C_s/C_L < 1$, which makes Mn segregates towards the interdendritic region. With these two opposite solid solute distribution, additional Mo content in 3xxx alloys could make it possible to obtain a more uniform distribution of the dispersoids and reduce the area of dispersoid free zone. Fig. 2.18 shows the EDS analysis of the as-cast Al-7Si-0.5Cu-0.3Mg-0.1Fe-0.3Mo-1.5Mn alloy, which indicate that Mo is segregated in the Al dendrite core while Mn is segregated in the interdendritic region[24].

TEM-EDS analysis shows that the Mo containing $\alpha - \text{Al}(\text{Fe}, \text{Mn}, \text{Mo})\text{Si}$ dispersoid phase has a stoichiometric formula of $\text{Al}_{22}(\text{Fe}_{1-3}\text{Mn}_{4-6}\text{Mo})\text{Si}_4$, and it is the only Mo-containing intermetallic that forms in the Al-7Si-0.5Cu-0.3Mg-0.1Fe-0.3Mo-1.5Mn alloy [24]. Also, the amount of the $\alpha - \text{Al}(\text{Fe}, \text{Mn}, \text{Mo})\text{Si}$ dispersoids increases with increasing Mn (Fig. 2.19) and has the similar atomic structure with $\alpha - \text{Al}(\text{Fe}, \text{Mn})\text{Si}$ phase, which is the main dispersoid phase in 3xxx alloys. On the basis of these results, the trace addition of Mo can be used on 3xxx alloys to get possible higher strength at elevated temperature.

3 Experimental procedure

3.1 Alloy preparation

The AA3004 alloys were prepared by commercial grade 1020 alloy and Al-50 % Si, Al-25 % Fe, Al-25 % Mn, pure Mg and Al-10 % Mo master alloys. Master alloys were added into the liquid 1020 alloy to cast a series of AA3004 alloys with different amounts of Mo addition. The experimental alloys were synthesized in an electrical resistance furnace (Fig. 3.1) within a clay-graphite crucible and cast into a preheated (250°C) permanent mold. The dimension of cast ingots was 30mm×40mm×80mm. The chemical compositions of the alloys were analyzed using optical emission spectrometer (OES), as shown in Table 3.1.

Table 3.1 Chemical compositions of the experimental alloys

Alloy ID	Si	Fe	Mn	Mg	Mo	Al
Base	0.30	0.60	1.25	1.28	0	Bal.
M10	0.28	0.59	1.24	1.25	0.10	Bal.
M20	0.28	0.60	1.23	1.26	0.19	Bal.
M30	0.27	0.61	1.18	1.21	0.27	Bal.
M40	0.27	0.61	1.22	1.26	0.29 * (0.4% target)	Bal.
M50	0.27	0.59	1.20	1.25	0.35 * (0.5% target)	Bal.
M70	0.26	0.62	1.20	1.23	0.54 * (0.7% target)	Bal.

* Note: Due to the precipitation of primary AlMo intermetallic particles and non-uniform distribution of these particles in the liquid (see later Fig. 4.1), the Mo contents analyzed in those three alloys are mostly underestimated by OES samples. Because of no oxidation nature of Mo in liquid aluminum, the target Mo addition is believed to completely dissolve in liquid aluminum.



Fig. 3.1 Electrical resistance furnace

3.2 Heat treatments

All the heat treatments were processed in an electrically resistance furnace with air-circulating chamber (Fig. 3.2), the heating rate is controlled at $4^{\circ}\text{C}/\text{min}$ ($240^{\circ}\text{C}/\text{h}$). The samples were immediately quenched into water at room temperature after heat treated. In order to evaluate the precipitation behavior of dispersoids, and get the optimal elevated temperature properties of AA3004 alloys, cast samples were treated at different temperature with different time and all the heat treatment is listed in Table 3.2.



Fig. 3.2 Electrically resistance air-circulating chamber furnace

Table 3.2 Heat Treatment Conditions in present project

No.	Conditions
(A)	600°C , 550°C , 525°C, 500°C,475°C×0-24h
(B)	375°C , 425°C×0-96h
(C)	375°C × 48h+ 500°C ×0-12h
(D)	175°C , 250°C, 330°C × 0-72h+ 375°C × 48h

Group A and B are single-step precipitation treatment, which was designed to study the precipitation behavior of dispersoids at different precipitation temperature and time. Different temperature from 375°C to 600°C was applied, and different time from 0 to 96 hours were

also performed to find both the optimized precipitation temperature and time for the precipitate of dispersoids as well as the influence of Mo addition. Group C and D are two-step precipitation treatment, in which the precipitation treatment was consist of two treatments in different temperature. Group C was focused on the study of the dispersoid coarsening. The first step precipitation treatment at 375°C for 48 hours was applied to get a large volume fraction of fine dispersoids while the second step treatment at 500°C will cause the coarsening of the dispersoids. Group D applied additional preheating treatments as the first step treatment before the precipitation treatment at 375°C for 48 hours. The preheating treatments are to get possible more nucleus for dispersoids and then get more uniformly distributed and finer dispersoids, which could have significant improvement on alloys' properties. Different temperature from 175°C to 330°C was applied.

3.3 Microstructure observation

The microstructure is observed by optical microscope (OM) (Fig. 3.3), Scanning Electron Microscope(Fig. 3.4) and Transmission Electron Microscope(Fig. 3.5) respectively. The metallographic specimens are grinded and polished to the desired fine finish by a Struers Tegrapol-35 Grinder-Polisher(Fig. 3.5). For OM observation, etching technology (0.5%HF for 30 seconds) are used for the analysis of distribution of dispersoids. The area fraction of DFZ is calculated by using the Clemex PE 4.0 image analysis software. A scanning electron

microscope (SEM, JSM-6480LV) equipped with an energy dispersive x-ray spectrometer (EDS) is used to observe the casted samples to determine the microstructure and chemical composition of the intermetallic particles in the alloys. A transmission electron microscope (TEM, JEM-2100) operated at 200kV is also applied to identify the dispersoids as well as the characters of dispersoids, such as size and volume fraction.



Fig. 3.3 Optical microscope



Fig. 3.4 JSM-6480LV Scanning Electron Microscope



Fig. 3.5 JEM-2100 Transmission Electron Microscope



Fig. 3.6 Struers Tegrapol-35 Grinder-Polisher

3.4 Electrical conductivity

The electrical conductivity (EC) is performed to evaluate the solute levels in Al matrix for alloys in all as-cast and heat-treated conditions. Electrical conductivity is measured on ground samples using a portable FISCHER SIGMASCOPE® SMP 10 Electrical Conductivity Measurement System (Fig. 3.7). The electrical conductivity was measured at room temperature in terms of percentage of international annealed copper standard (%IACS). Minimum six readings were taken for each sample and then the average value was calculated for plotting the graph of electrical conductivity versus treating time. Before conducting electrical conductivity test, the equipment is calibrated on standards of known conductivity. The measured values were considered to be accurate within ± 0.5 %IACS.



Fig. 3.7 Portable FISCHER SIGMASCOPE® SMP 10 Electrical Conductivity Measurement System

3.5 Microhardness

The microhardness tests are performed on all the samples using a NG-1000 CCD Vickers microhardness test machine(Fig. 3.8) with a load of 200g and a dwell time of 20s at room temperature. All the Microhardness data are obtained on polished samples and the locations of indentation were on the aluminum matrix to determine the influence of dispersoids precipitation on hardness. The average value of 12 measurements was recorded for each sample.



Fig. 3.8 NG-1000 CCD microhardness test machine

3.6 Mechanical properties test

The mechanical property test, which is compressive yield strength in this research, is obtained from compression tests performed on a Gleeble 3800 machine (Fig. 3.9). Cylindrical specimens with a 15 mm length and 10 mm diameter are machined and tested at elevated temperature (300°C) following the ASTM E9-89a standard. The total deformation of the specimens are set to 0.2 while the strain rate is fixed at 10^{-3}s^{-1} . The specimen is heated to 300°C with a heating rate of 2°C/s and hold for 3 minutes to stabilize. An average value of YS is obtained from 3 tests. In addition, creep tests are performed at 300°C for 100 hours on some selected conditions. Creep specimens are the same size as the Gleeble samples. Creep tests are conducted under compression with a constant load of 45 MPa. For each condition, an average value of data is obtained from 3 tests.



Fig. 3.9 Gleeble 3800 machine

4. Results and Discussion

4.1 Effect of Mo additions on as-cast properties

The measurements of as-cast properties with various Mo additions, including microhardness, electrical conductivity(EC) as well as microstructure observation were performed for all the alloys (the base 3004 alloy and Mo-containing alloys) to verify the effect of different Mo additions.

4.1.1 Microstructure

The as-cast microstructures of the base 3004 and Mo-containing alloys were observed by OM and SEM. Fig. 4.1 shows the optical micrographs of the alloys. After casting all the alloys have large amount of rod like, eutectic intermetallic particles, which are distributed in the interdendritic regions. Besides, there is no obvious difference on the microstructure between base 3004 and Mo-containing alloys when the Mo content is lower than 0.3%. However, Mo-containing intermetallic particles can be found when Mo content is higher than 0.4%(Fig. 4.1e). For M50 and M70 alloys, as shown in Fig. 4.1f and 4.1g, there were a lot of large primary Mo-containing intermetallic particles. According to the literature [23], these Mo-containing primary particles are formed during the solidification when the amount of Mo content exceeded the maximum liquid solubility, which is about 0.08wt% in Al at 660°C,

however, as the maximum solid solubility of Mo in Al matrix is 0.25wt%, after solidification, there could be a reasonable amount of Mo content in the Al solid solution without forming primary particles. .

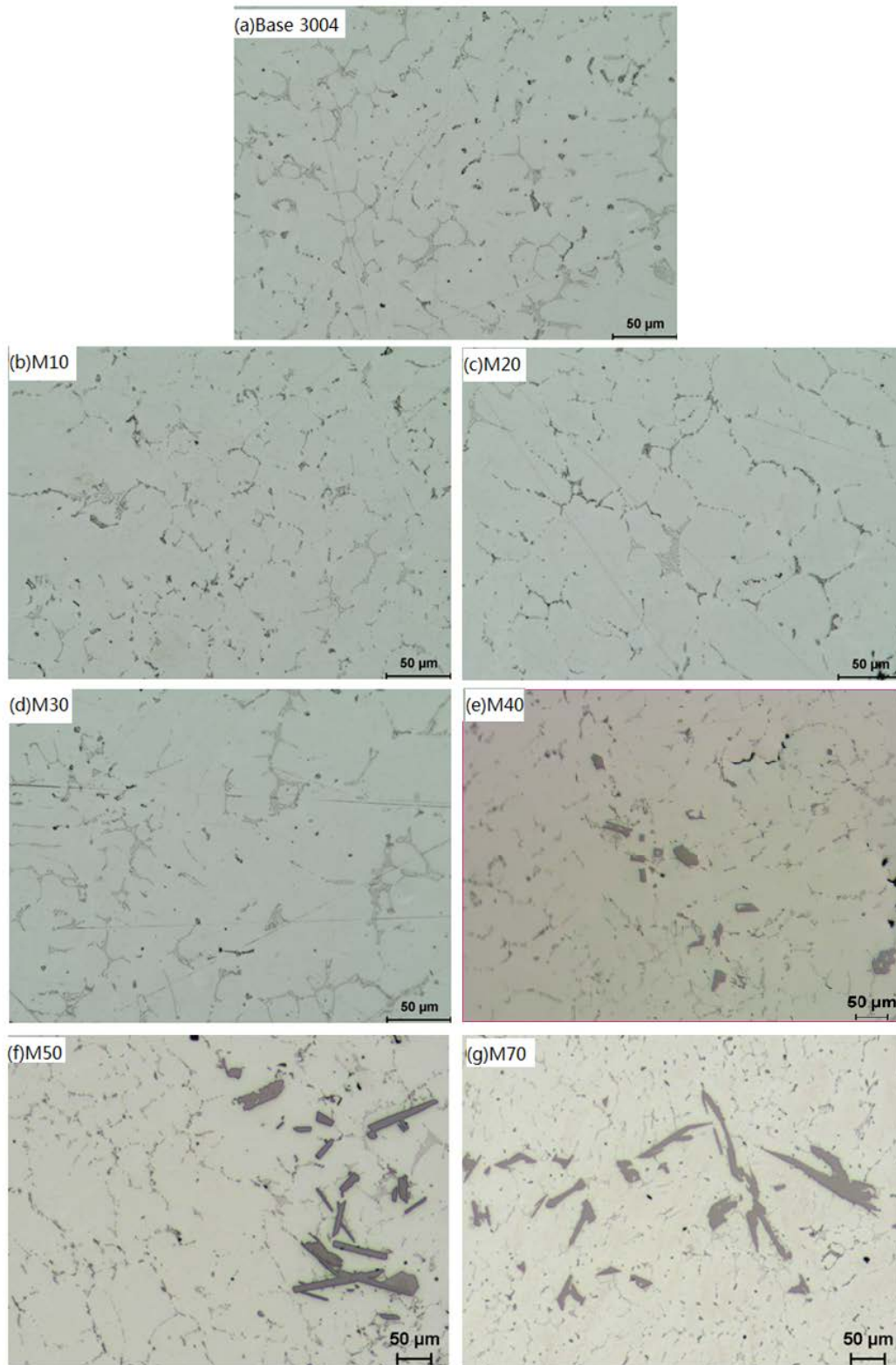


Fig. 4.1 As-cast microstructure of (a) the base 3004 alloy; (b) M10; (c) M20; (d) M30; (e) M40; (f) M50;

(g) M70

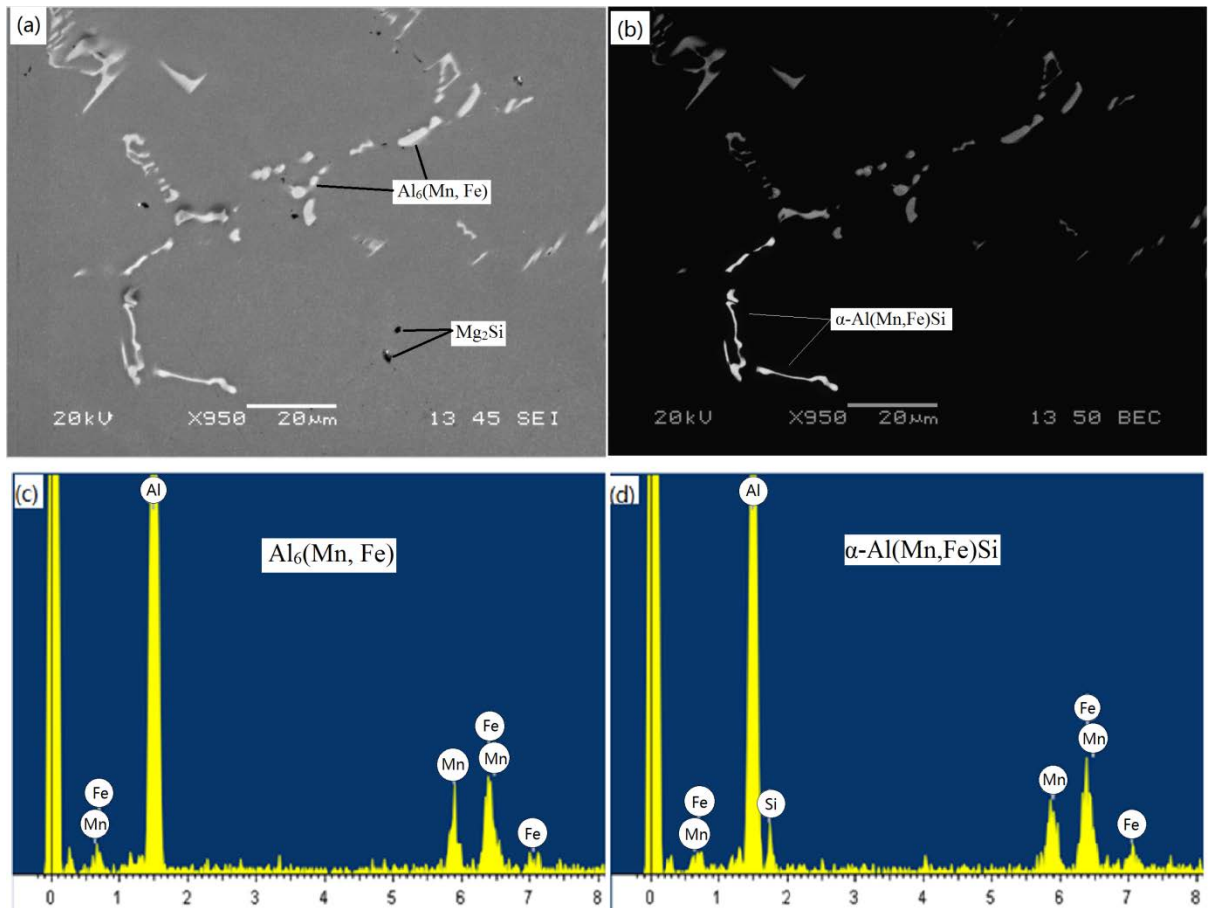


Fig. 4.2 SEM image of the base 3004 alloy (a-b) and SEM-EDS results(c-d)

Fig. 4.2 shows the SEM image of the as-cast base 3004 alloy. Most of the intermetallic particles are gray $Al_6(Mn, Fe)$ intermetallic phase, and some black Mg_2Si as well as the small amount of $\alpha-Al(Mn, Fe)Si$ is also observed, which is the brighter phase than $Al_6(Mn, Fe)$ in the SEM backscattered mode due to the presence of Si element. Fig. 4.3 shows the SEM image of the as-cast M30 and M40 alloys. It can be found that the distribution of the intermetallic phases in M30 alloys are similar with the base 3004 alloy. Also, the chemical composition of these intermetallic particles were analysed by EDS, little of them contains Mo element, which means that most of the Mo content were in the solid solution after solidification. However,

some primary Mo-containing intermetallic particles have been observed in M40(Fig. 4.3b), which could be deleterious to the alloy properties and should be avoid during solidification or dissolved during heat treatment.

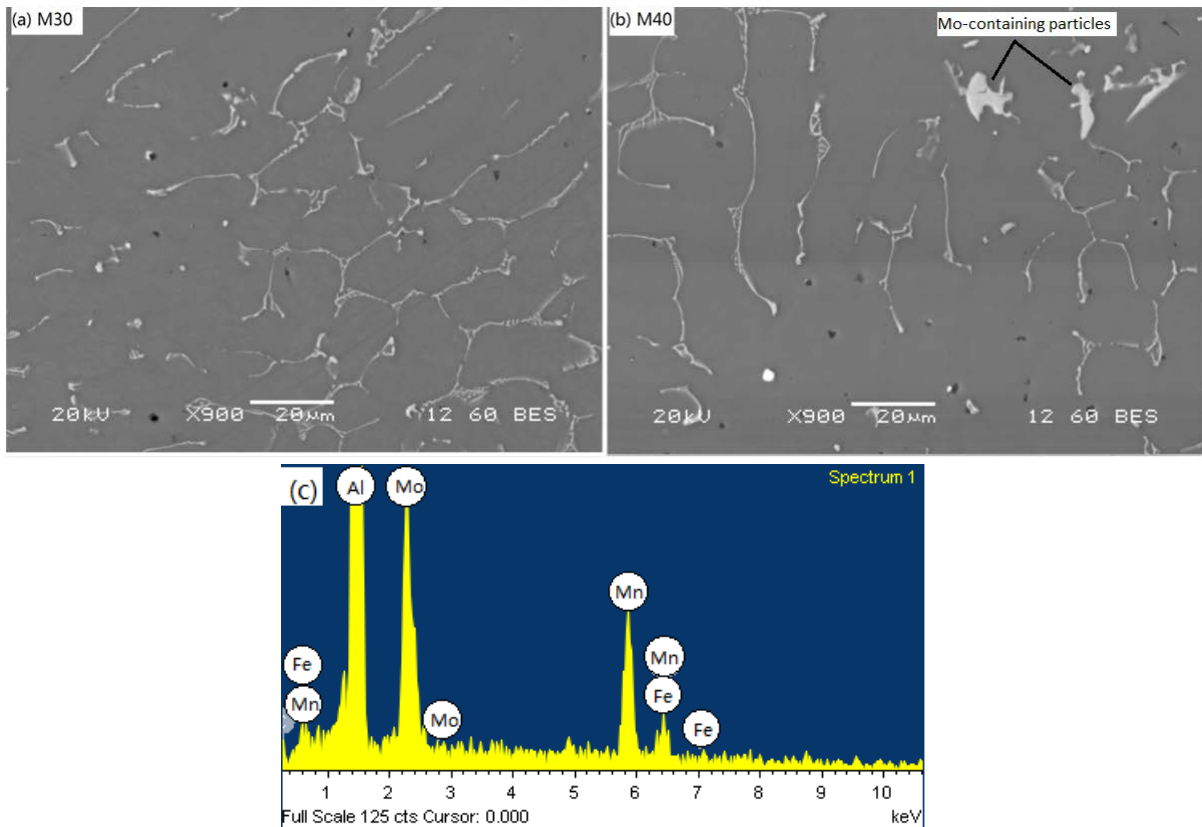


Fig. 4.3 SEM image of (a)M30 and (b)M40 SEM-EDS results (c) for Mo-containing particles

The homogenization treatment was applied to the M50 alloy to try to dissolve the Mo-containing primary particles and create a higher solid solution of Mo atoms in the matrix. The homogenization samples were first polished and observed by optical microscope to get the images of the microstructure where those Mo-containing primary particles located. Then the samples were homogenized at 600°C for 24 hours. After the homogenization treatment, the samples were slightly polished to remove the oxide layer without destroying the original surface and observed at the same position to find out whether the specific primary particles were dissolved. The results were shown in Fig. 4.4.

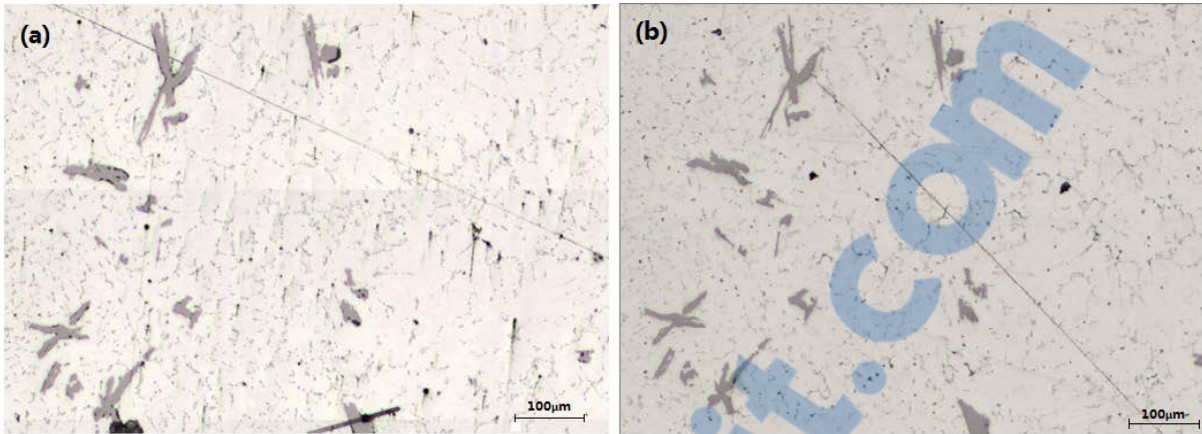


Fig. 4.4 Optical Microstructure of M50 alloy (a) As-cast; (b) 600°C× 24h

It can be found that all those primary particles did not have any significant change in both the size and the shape after 24 hours homogenized at 600°C. The Al-Mo binary phase diagram (Fig. 2.15) indicated that these Mo-containing primary particles are the peritectic particles that formed prior to the solidification of the Al dendrites, which was very hard to dissolve by homogenization treatment. Therefore the best way to avoid the formation of these particles is controlling the amount of the Mo addition (<0.4 %).

4.1.2 Microhardness and electrical conductivity

The EC measurements are used to determine the amount of solute in solid solution. In AA3xxx alloys their relationship can be expressed as [10, 11, 16, 38]:

$$1/EC = 0.0267 + 0.032Fe_{ss}\% + 0.033Mn_{ss}\% + 0.0068Si_{ss}\% + 0.003Mg_{ss}\% + 0.0021particle\%$$

Where $Fe_{ss}\%$, $Mn_{ss}\%$, $Si_{ss}\%$ and $Mg_{ss}\%$ and $particle\%$ are weight percentage. As shown in the equation, Si_{ss} , Mg_{ss} and $particle$ percentages have much less effect on EC than Mn_{ss} and

Fe_{ss} . Meanwhile, most of Fe was in the form of intermetallics during solidification, such as $Al_6(MnFe)$ and $\alpha-Al(MnFe)Si$. Therefore, the changes of EC during precipitation treatment primarily depended on the concentration of Mn in solid solution in AA3xxx alloys. In this research, Mo is another principal solute element and also influences the EC. From the EC data of as-cast condition in Fig. 4.5, the base 3004 alloy has the highest EC among the alloys, as there is no Mo content in base 3004 alloy. The EC of the alloys decreases with increasing amount of Mo content, and has the minimum value at 0.4% and then increases a bit with higher Mo content. The decrease of the EC indicates that there is more Mo in the solid solution with higher Mo contents. When the Mo content reaches 0.4%, the amount of Mo exceed the maximum solubility, the EC gets the lowest value. With further increasing Mo content, the Mo-containing primary particles start to form, consuming more Mo and leading to the slight increase of the EC values.

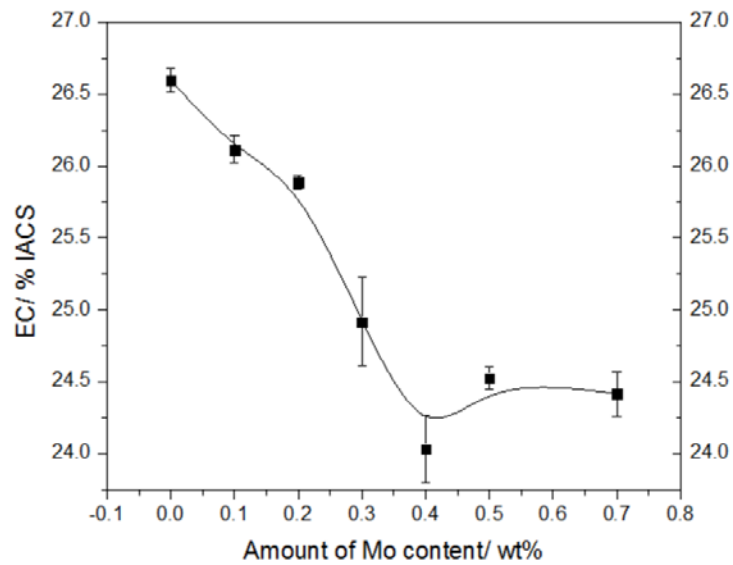


Fig. 4.5 Electrical conductivity of as-cast alloys

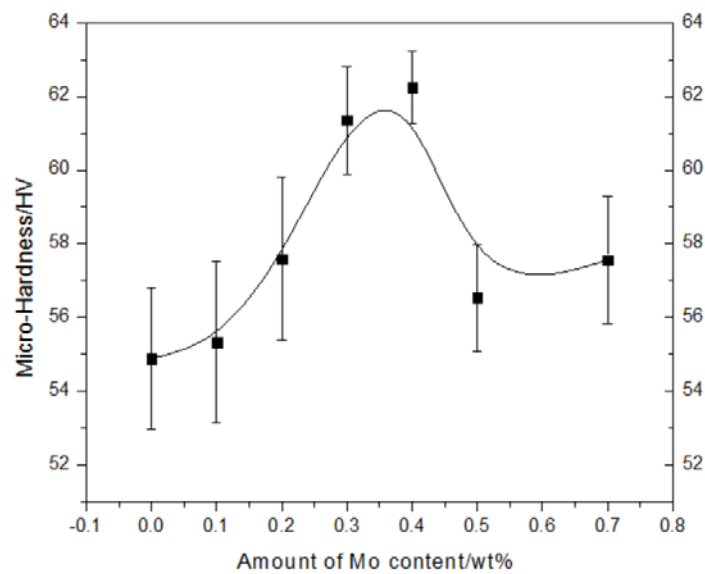


Fig. 4.6 Microhardness of as-cast alloys

Fig. 4.6 shows the microhardness results of various alloys. At the as-cast condition, there is very few dispersoids formed in the alloys, thus the hardness change is basically contributed by the solid solution strengthening. The hardness results indicated that Mo content can provide considerable solution strengthening effect since all the Mo-containing alloys have

higher microhardness than base 3004 alloy. First, the microhardness increases with increasing amount of Mo content, and gets the maximum value at 0.4%Mo. After the peak value, the microhardness decreases with increasing Mo content. The microhardness evolution as a function of Mo content is similar with the EC result. The increase of the microhardness at the beginning is caused by the increasing Mo solutes in the solid solution. When the Mo content is large than 0.4% and excesses the maximum solubility in aluminum, the microhardness drops with the formation of Mo-containing primary particles. The formation of the Mo-containing primary particles consumes the Mo solutes in the solid solution, weakening the solid solution strengthening and thus have negative effects on the mechanical properties including hardness and yield strength. Therefore these primary particles are not desirable and should be avoided or eliminated. Since the homogenization treatment is proved not be able to dissolve the primary Mo-containing particles, the best way to avoid these particles is to control the amount of Mo content. Since M30 alloy has no primary Mo-containing particles and also possess much higher microhardness than base 3004 alloy, 0.3%Mo content is considered to be the optimal Mo content in AA3004 alloy.

4.2 Evolution of microstructure and properties during heat treatment

The recent researches showed that in 3xxx alloys, a reasonable amount of α -Al(Mn,Fe)Si dispersoids can be precipitated around 375°C to 425°C[5, 9, 11, 12], while Mo

containing dispersoids may form after treated around 540°C in Al-Si cast alloy[23, 24]. The precipitation treatments are divided into two groups: low temperature and high temperature precipitation treatments (Table 3.2), to study the precipitation behaviour of dispersoids and the influence of Mo addition in AA 3004 alloys.

4.2.1 Microstructure evolution during precipitation treatment

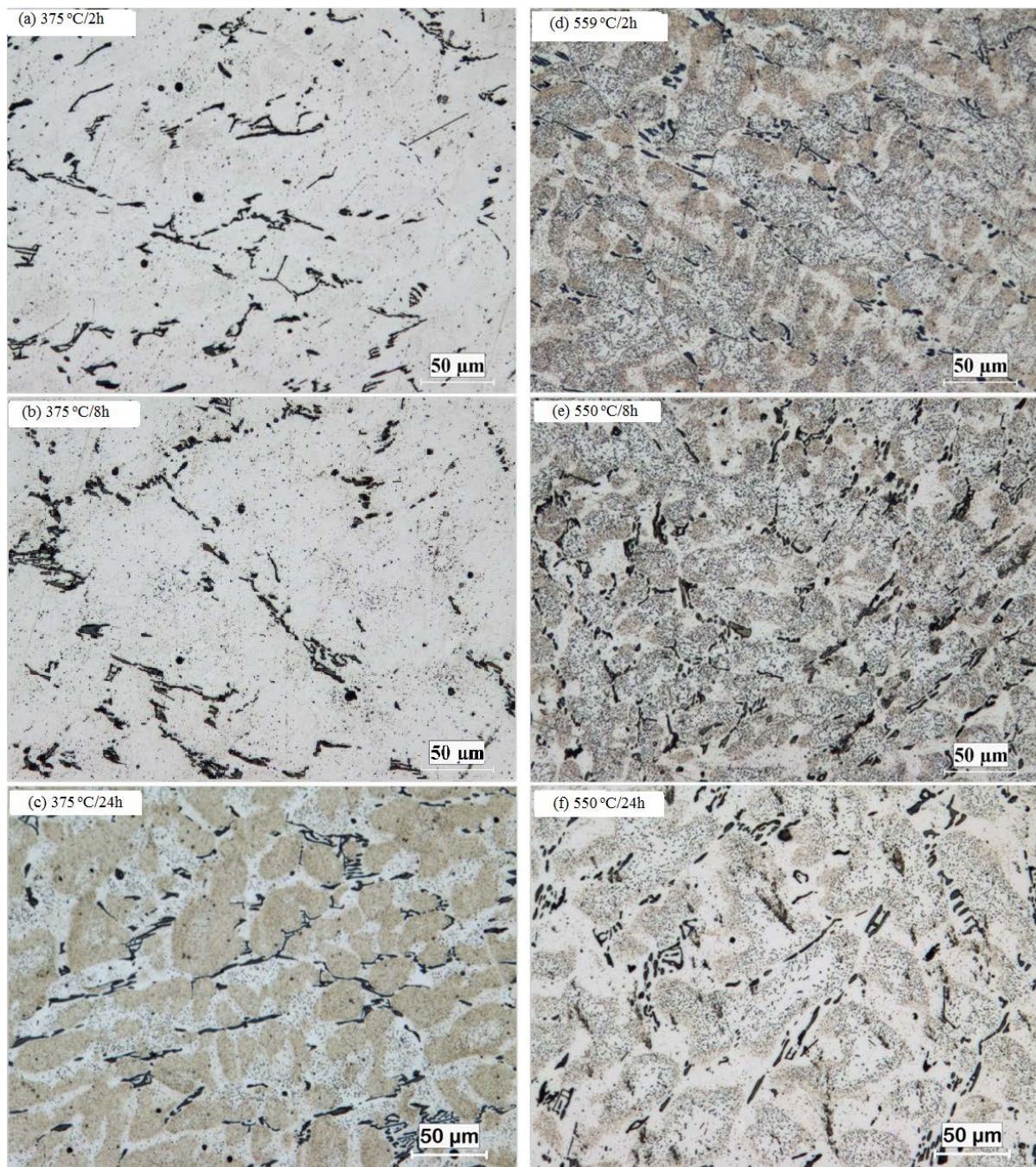


Fig. 4.7 Microstructure evolution during precipitation treatment for base 3004 alloy (a) 375°C/2h; (b) 375°C/8h; (c) 375°C/24h; (d) 550°C/2h; (e) 550°C/8h (f) 550°C/24h, etched with 0.5% HF for 30s.

In order to study the precipitation behavior for base 3004 and M30 alloys during precipitation treatments, especially the influence of temperature and time, the alloys are treated at different precipitation temperatures from 375°C to 600°C for up to 24 hours. After precipitation treatment, the samples are water quenched to room temperature and then polished and etched with 0.5%HF and observed by both the OM and SEM. The etched samples can also show the distribution of the dispersoids and DFZ. The distribution of the dispersoids and DFZ has significant influence on the properties of the alloys. Generally, the alloy will have better property when there are more and finer uniformly distributed dispersoids and less DFZ.

Fig. 4.7 showed the microstructure evolution during precipitation treatment for base 3004 alloy at 375°C and 550°C. From Fig. 4.7a-c it can be found that after 2 and 8 hours treatments at 375°C, there were few dispersoids precipitated. As the treatment time increases, the amount of the dispersoids increased. After 24 hours treatment, there were a large amount of fine and uniformly distributed dispersoids locate in the aluminum matrix. The particle free zones(DFZ) also appeared within the intradendritic regions and in the regions around the intermetallic particles. Meanwhile, for the precipitation treatment under 550°C (Fig. 4.7d-f), because of the high diffusion rate of Mn, the dispersoids precipitated much faster. After 2 hours treatment, there were already a large amount of dispersoids precipitated, the distribution of the dispersoids is similar with 375°C but the size of the dispersoid is larger with lower number

density. Furthermore, with the increasing treating time, the dispersoids became coarse and the number density decreases. The size of the dispersoid became larger, some of the dispersoids dissolved into the aluminum matrix after 24 h at 550°C (Fig. 4.7f), resulting in enlarged DFZ.

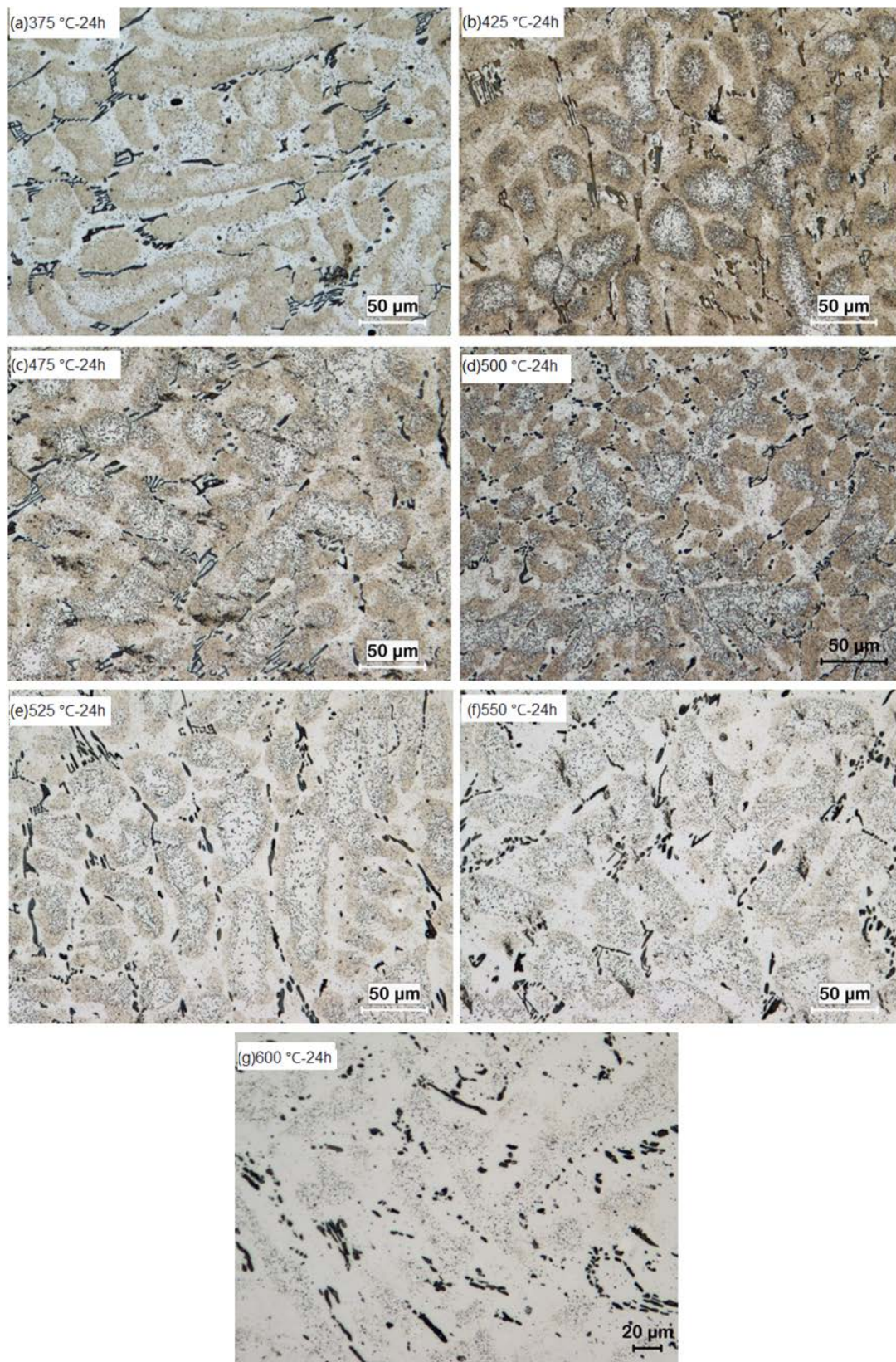


Fig. 4.8 Microstructure evolution of base 3004 alloy for different precipitation temperatures, etched with

0.5%HF for 30s.

Fig. 4.8 and Fig. 4.9 showed the microstructure evolution for base 3004 and M30 alloys under different precipitation temperatures for 24 hours. The microstructure of base 3004 alloy treated at 375°C for 24 hours was shown in Fig. 4.8a, the dispersoid zones are presented as the dark gray regions, the white regions are DFZ. After treated at 375°C for 24 hours, a high volume of dispersoids formed in the dendrite cells. However, there were some DFZ surrounding the intermetallic particles and in the intradendritic regions. The DFZ surrounding the intermetallic particles is formed by the depletion of Mn content due to the formation of $\text{Al}_6(\text{Mn,Fe})$ intermetallic particles during solidification in the interdendritic regions. The formation of $\text{Al}_6(\text{Mn,Fe})$ intermetallic particles absorbed the Mn content and resulted in low Mn concentration in areas nearby. On the other hand, the DFZ in the intradendritic regions is caused by the microsegregation of Mn ($K_0 < 1$) during solidification. The low Mn concentration in the centers of the dendrites makes the precipitation of dispersoids more difficult. With the increasing precipitation temperatures (Fig. 4.8b-g), the dispersoids become less and coarser, and the DFZ became wider and larger.

The evolution of dispersoids during precipitation treatment is highly related with the diffusion of Mn in aluminum matrix. At low precipitation temperature, like 375°C and 425°C, with the decomposition of supersaturated Mn solid solution, the dispersoids nucleate and growth in Al matrix. Due to the low Mn diffusion rate at these temperature (the diffusion rate

of Mn at 400°C is about $1.35 \times 10^{-3} \mu\text{m}^2/\text{h}$ [2], the long distance diffusion of Mn is nearly impossible. Thus continuous precipitation of fine dispersoids is dominant, while the influence of coarsening on the dispersoids is less. However, the diffusion rate of Mn in the Al matrix has increased significantly with increasing temperature, and then the precipitation of dispersoids is much faster and the coarsening became the dominant mechanism. Meanwhile, higher temperature means higher solid solubility of Mn in Al matrix, which caused the dissolve of the dispersoids. In the intradendritic regions, the dissolve and the coarsening of the dispersoids caused enlarged DFZ area. When the temperature is higher than 525°C, long distance diffusion between dispersoids and intermetallic particles can occur with higher diffusion Mn rate. The eutectic networks of $\text{Al}_6(\text{Mn,Fe})$ intermetallic begin to break up, and the large $\text{Al}_6(\text{Mn,Fe})$ intermetallic fragmented into disconnected small parts, the fragment effect make the intermetallic particles became coarser. The dispersoids surrounding the $\text{Al}_6(\text{Mn,Fe})$ intermetallic particles dissolved due to the coarsening of the $\text{Al}_6(\text{Mn,Fe})$ intermetallic particles. This phenomena explained the enlarged DFZ surrounding the $\text{Al}_6(\text{Mn,Fe})$ intermetallic particles with increasing temperature.

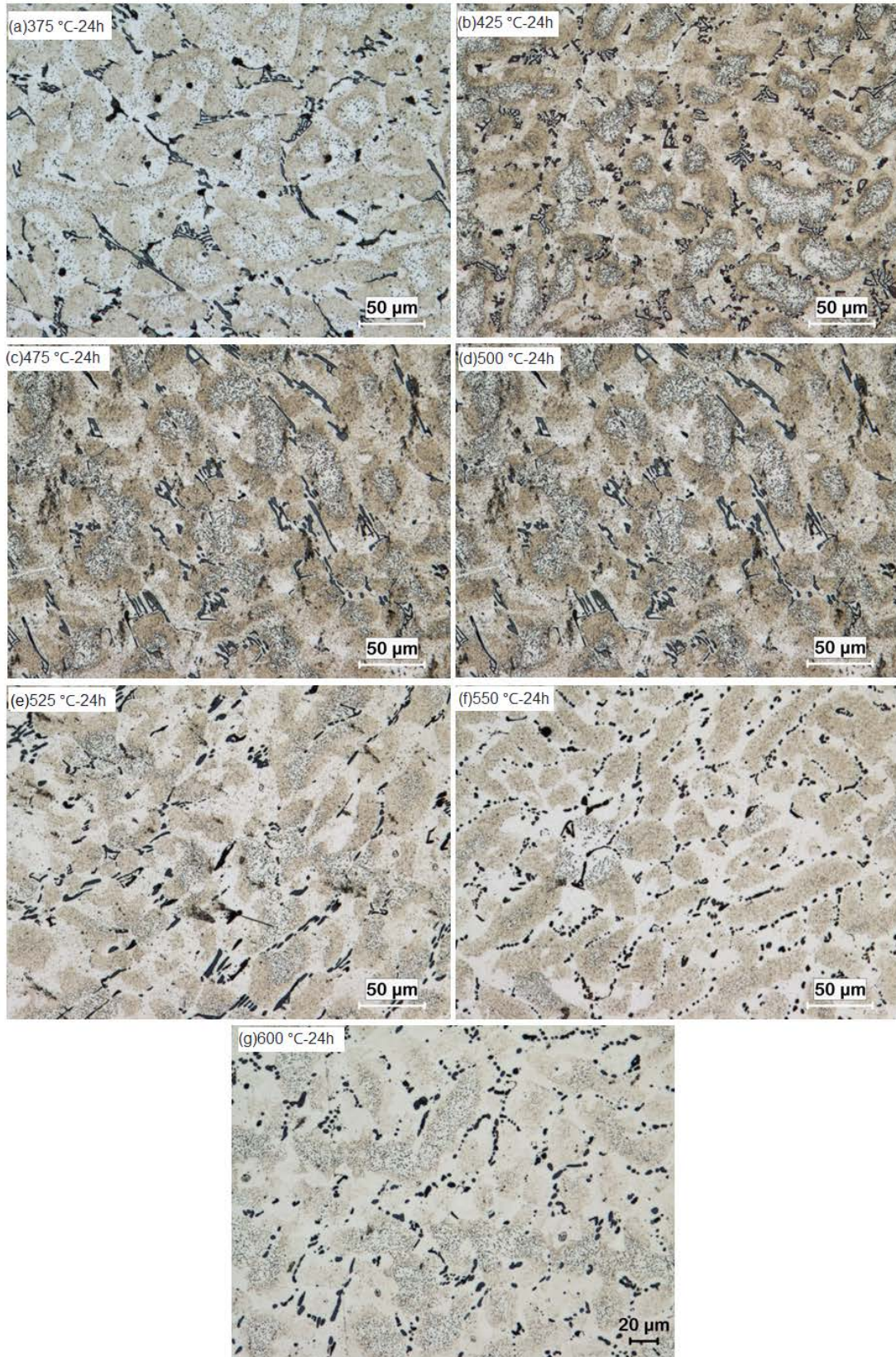


Fig. 4.9 Microstructure evolution of M30 alloy for different precipitation temperatures, etched with

0.5%HF for 30s.

The microstructure evolution of M30 alloys during precipitation treatment at different temperatures is shown in Fig. 4.9. At 375°C and 425°C, the distribution of dispersoids and DFZ of M30 alloy have no significant different with base 3004 alloy. But with increasing temperature, M30 alloy has significant more dispersoids with smaller and less DFZ regions, especially in the intradendritic regions. When the precipitation temperature is higher than 500°C there are still reasonable amount of uniformly distributed dispersoids located in the intradendritic regions, and the DFZ can only be found surrounding the $Al_6(Mn,Fe)$ intermetallic particles in M30 alloys. This significant difference of dispersoids distribution is contributed by Mo addition. Mn has a solid-liquid partition coefficient, $k_0 = C_s/C_L < 1$, which makes Mn segregates towards the interdendritic region. While Mo as a peritectic element, has $k_0 = C_s/C_L > 1$ which makes Mo segregates towards the intradendritic regions. With these two opposite solid solute distribution, additional Mo content helps 3004 alloy to obtain a more uniformly distributed dispersoids and reduce the area of DFZ by providing more solute concentration in intradendritic regions.

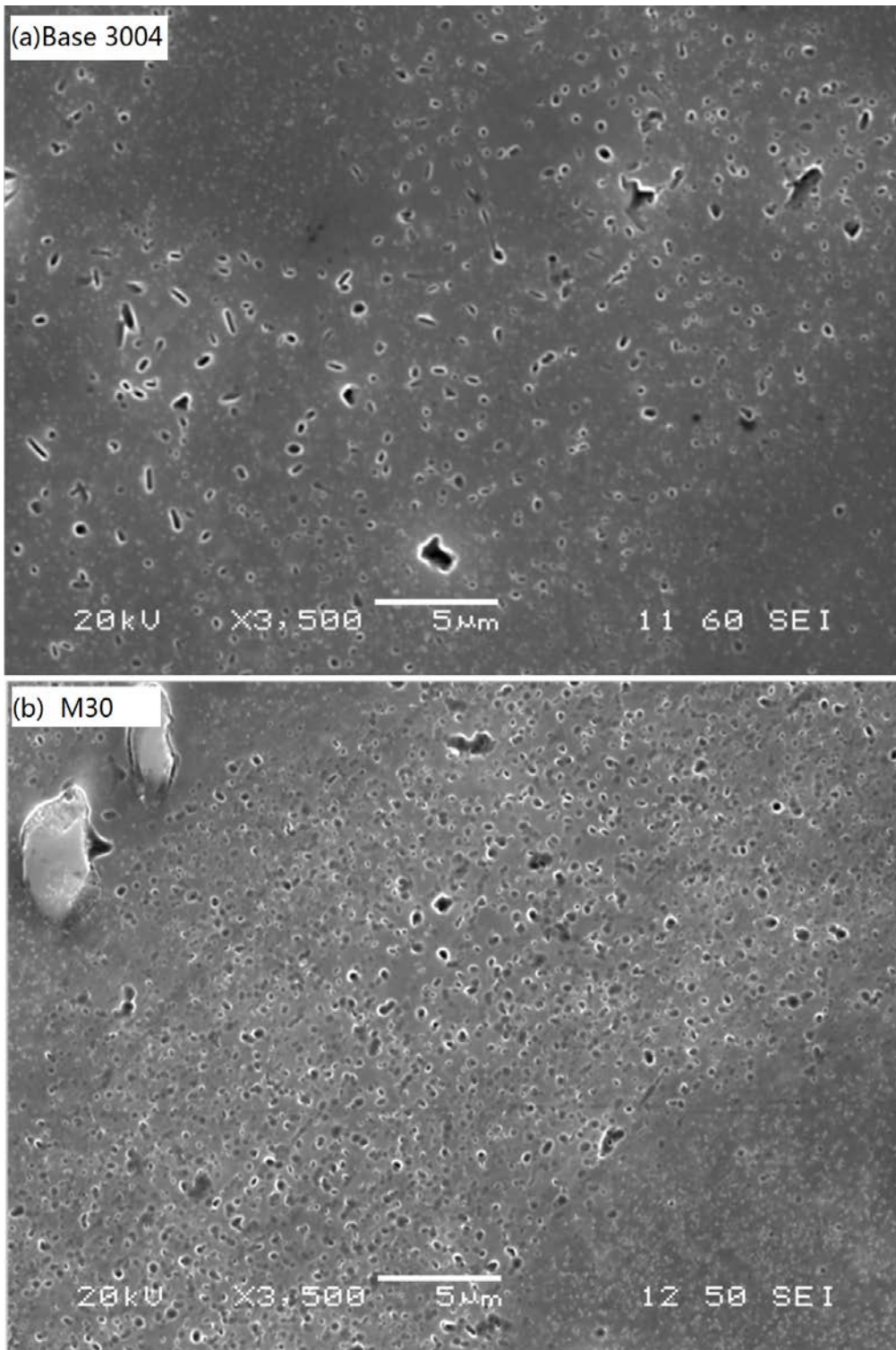


Fig. 4.10 The SEM image of the dispersoids of (a) base 3004 alloy and (b) M30 alloy after treated at 550°C for 24 hours

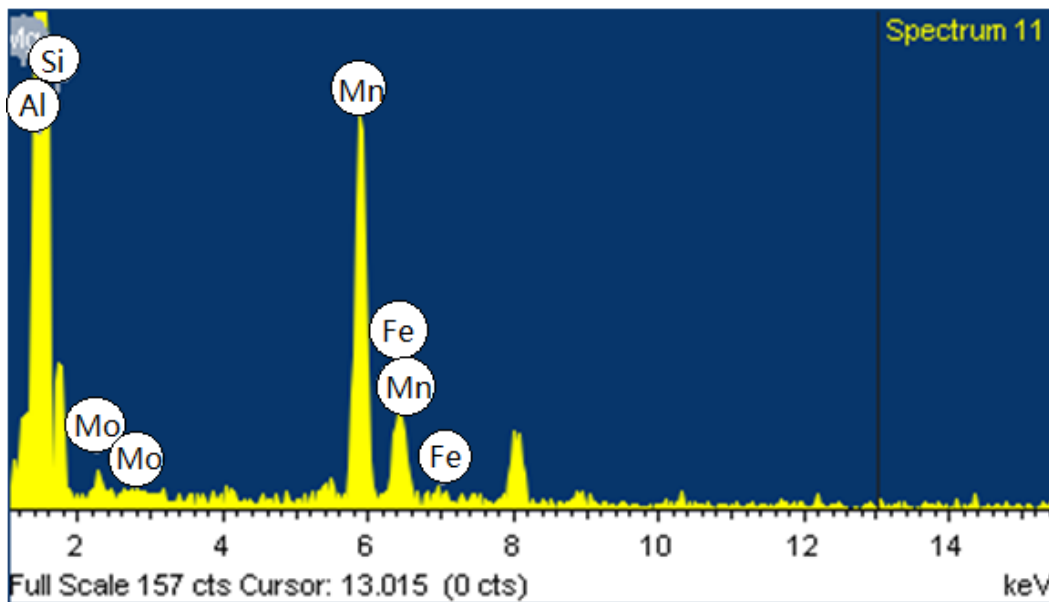


Fig. 4.11 TEM-EDS spectrum of the dispersoids in M30 alloy after treated at 550°C for 12 hours

Fig. 4.10 shows the SEM image of the dispersoids for base 3004 alloy and M30 alloy after treated at 550°C for 24 hours. M30 alloy formed significantly more and finer dispersoids in intradendritic regions than base 3004 alloy. The size of the dispersoids in base 3004 alloy is much larger than the dispersoids in M30 alloy, while the number density is much lower.

The TEM-EDS spectrum(Fig. 4.11) shows that the dispersoids seems to be α -Al(Mn,Fe,Mo)Si. It is similar with α -Al(Mn,Fe)Si dispersoids in the base alloy, in which Mo replaces with Mn and Fe each other. The α -Al(Mn,Fe,Mo)Si dispersoids have been reported to have a significant improvement in the YS, UTS and creep resistance by effectively pinning the dislocations in the dendrite grain interiors and delay the void nucleation and growth[23]. Meanwhile, the existence of Mo in α -Al(Mn,Fe,Mo)Si dispersoids could

increase the coarsening resistance of the dispersoids[24]. It has been reported that the dissolution of alloying elements with low diffusion rate in the dispersoid phase can decrease the growth rate constant(Mo has an diffusion rate of $2.3 \times 10^{-26} \text{m}^2/\text{s}^{-1}$ at 300°C [39]. Additionally, the low growth rate constant of the dispersoids can also result in less DFZ[40].

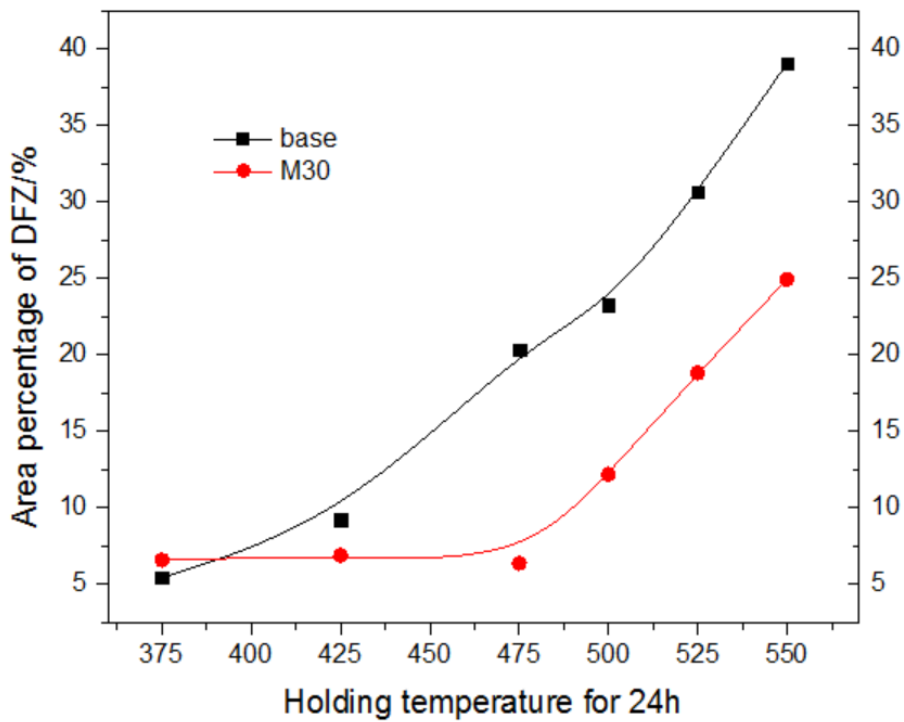


Fig. 4.12 Area percentage of DFZ after 24 hours precipitation treatment at different temperatures

The area percentages of DFZ after 24 hours precipitation treatment at different temperatures were measured using Clemex PE 4.0 image analysis software on the optical images and the results are shown in Fig. 4.12. The area percentage evolution of DFZ between base 3004 alloy and M30 alloy is significantly different. With increasing temperature, the area percentage of DFZ for base 3004 alloy increased sharply. For instance, after 24 hours

precipitation treatment at 550°C, the area percentage of DFZ reached as high as of 40%. As for M30 alloy, the area percentage of DFZ was low and stabled at around 7% from 375°C to 475°C. When the temperature was higher than 500°C, the area percentage of DFZ started to increase. After 24 hours precipitation treatment at 550°C, the area percentage of DFZ was around 25%, which was much lower than the base 3004 alloy. The lower area percentage of DFZ in M30 alloy is contributed to the more and finer dispersoids locate in the intradendritic regions, which is provided by the Mo addition.

4.2.2 Effect of Mo on the evolution of properties during precipitation treatments

Alloys containing different Mo contents, from 0 to 0.3% (Base, M10, M20, M30) were used to study the effect of Mo content during precipitation treatment. Fig. 4.13 and Fig. 4.14 showed the electrical conductivity and microhardness evolution during precipitation treatment at 375°C up to 48 hours and 550°C up to 24 hours. The results showed that Mo addition in 3004 alloy has positive strengthening effects during precipitation treatment at both low and high temperatures and the strengthening effect is proportional to the Mo content.

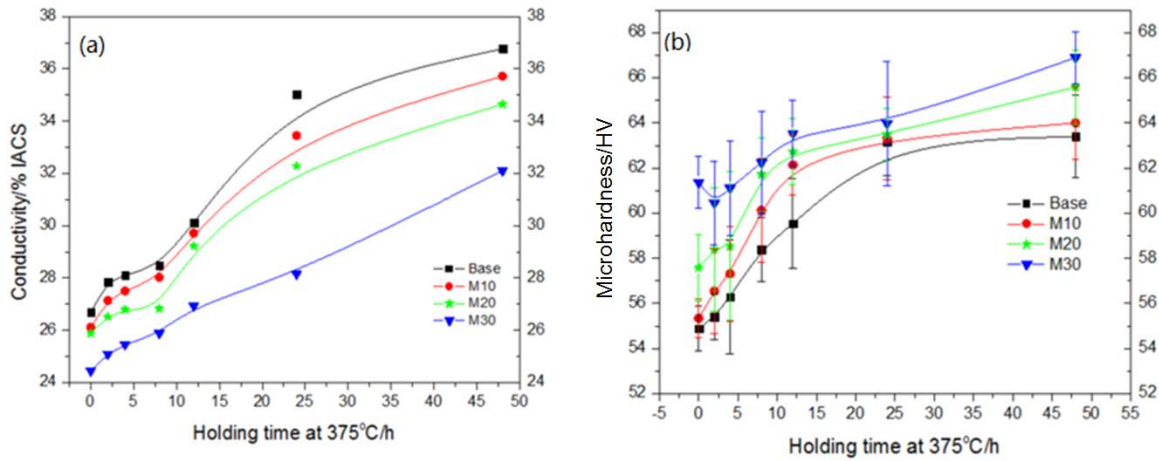


Fig. 4.13 Evolution of (a) electrical conductivity, and (b) microhardness for alloys with different Mo additions during precipitation treatment at 375°C

The evolutions of EC and microhardness of alloys with different Mo additions during precipitation treatment at 375°C are shown in Fig. 4.13. With increasing amount of Mo, from 0 to 0.3%, the value of EC decreases at any treatment time. For instance, base alloy has the highest EC since there is no Mo content while M30 alloy has the lowest EC with the highest Mo content in solid solution.

The EC of all those alloys increased with increasing holding time during precipitation treatment at 375°C. The increase of the electrical conductivity is caused by the decomposition of the Mn supersaturated solid solution during precipitation treatment and the formation of dispersoids. With the increasing holding time, the amount of dispersoids increased, which can provide strengthening effect to the alloy[5, 9, 12]. The increase of the microhardness during precipitation treatment reflects the effect of dispersoids on mechanical properties. The microhardness get the maximum value after 48 hours treatment. The difference of both EC

and microhardness between these alloys during precipitation treatment reveals that the Mo could provide strengthening effect at 375°C by both solid solution strengthening and α -Al(Mn,Fe,Mo)Si dispersoid strengthening. The alloy with higher microhardness during precipitation treatment contains higher content of Mo.

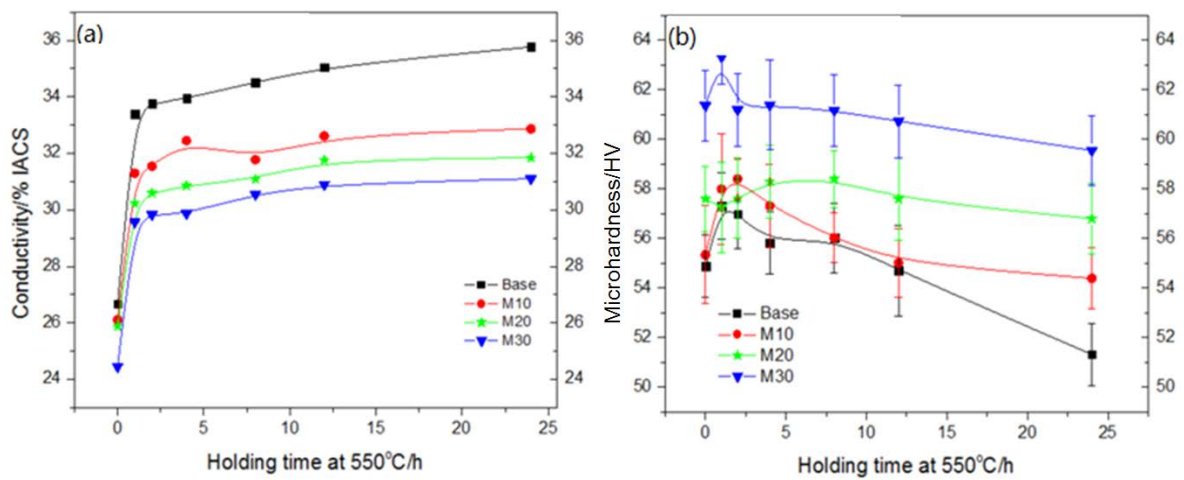


Fig. 4.14 Evolution of electrical conductivity (a) and microhardness (b) for alloys with different Mo

additions during precipitation treatment at 550°C.

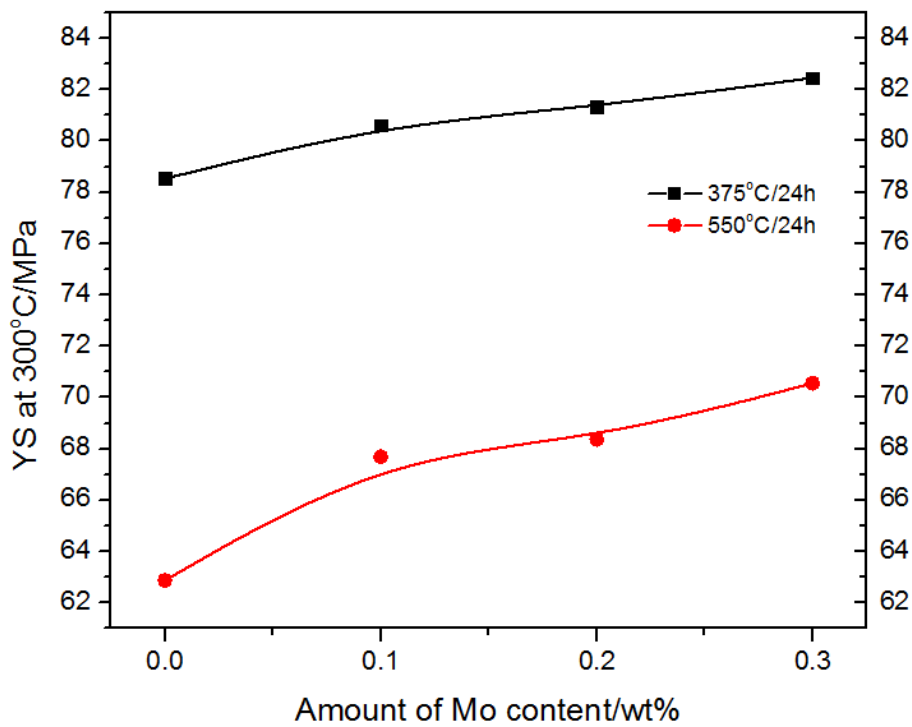


Fig. 4.15 YS at 300°C for alloys different Mo content after precipitation treatment

Fig. 4.14 shows the EC and microhardness evolutions during the precipitation treatment at 550°C. Fig. 4.14a shows the electrical conductivity evolution: all the alloys have a sharp increase of the EC during the precipitation treatment at 550°C, and it quickly reaches the high value after only 1 hour. After that, the values of EC only slightly increased with increasing holding time. Because of the high precipitation temperature, the Mn has higher diffusion rate, which made the decomposition of the solid solution become faster, leading to the rapid increase of conductivity. From Fig. 4.14b, a quick increase of the microhardness occurs at the beginning of the precipitation treatment, and the peak value is reached for all the alloys after around 2 hours treatment. This increase of the microhardness is caused by the precipitation of

the dispersoids, and also, because of the high precipitation temperature, the high diffusion rate of Mn make dispersoids coarsen, leading to the decrease of the microhardness as the holding time increases.

The microhardness evolution of different alloys during the precipitation treatment at 550°C also indicated that Mo addition has both solid solution strengthening and dispersoid strengthening. The microhardness evolution of base 3004 alloy during treated at 550°C showed a significant decrease after 2 hours treatment. When the base alloy was treated for 24 hours, the microhardness decreased greatly, even lower than as-cast state. The strengthening effect of the dispersoids is weakened because of the coarsening effect in base 3004 alloy. However, the alloys containing Mo not only possessed a higher but also a more stabilized microhardness during the treatment. The decrease caused by extended treating time is less compared to base 3004 alloy. The result of YS at 300°C (Fig. 4.15) show that after precipitation treatment, Mo containing alloys had higher strength at elevated temperature, and the strengthening effect is proportional to the amount of the Mo content. After 375°C for 24h, the YS at 300°C is improved from 78MPa to 82MPa with 0.3% of Mo addition. Meanwhile, after high temperature precipitation treatment the improvement is more evident, after 550°C for 24h the YS at 300°C is 70MPa for M30 alloy while base alloy is 62MPa. The Mo addition provides more uniformly distributed fine dispersoids in the intradendritic regions after high temperature precipitation (shown in Fig. 4.10). And with the low diffusion rate of Mo, the

Mo-containing dispersoids coarsen slowly and keep their strengthening effect with extended treating time and higher treating temperature.

4.2.3 Effect of precipitation treatment parameters on the evolution of properties

All the results show that M30(0.3% of Mo) has the best strengthening effect during precipitation treatment. In order to simplify the experimental procedure, M30 alloy was used to study the influence of different temperatures and times of precipitation treatment in comparison with base 3004 alloy.

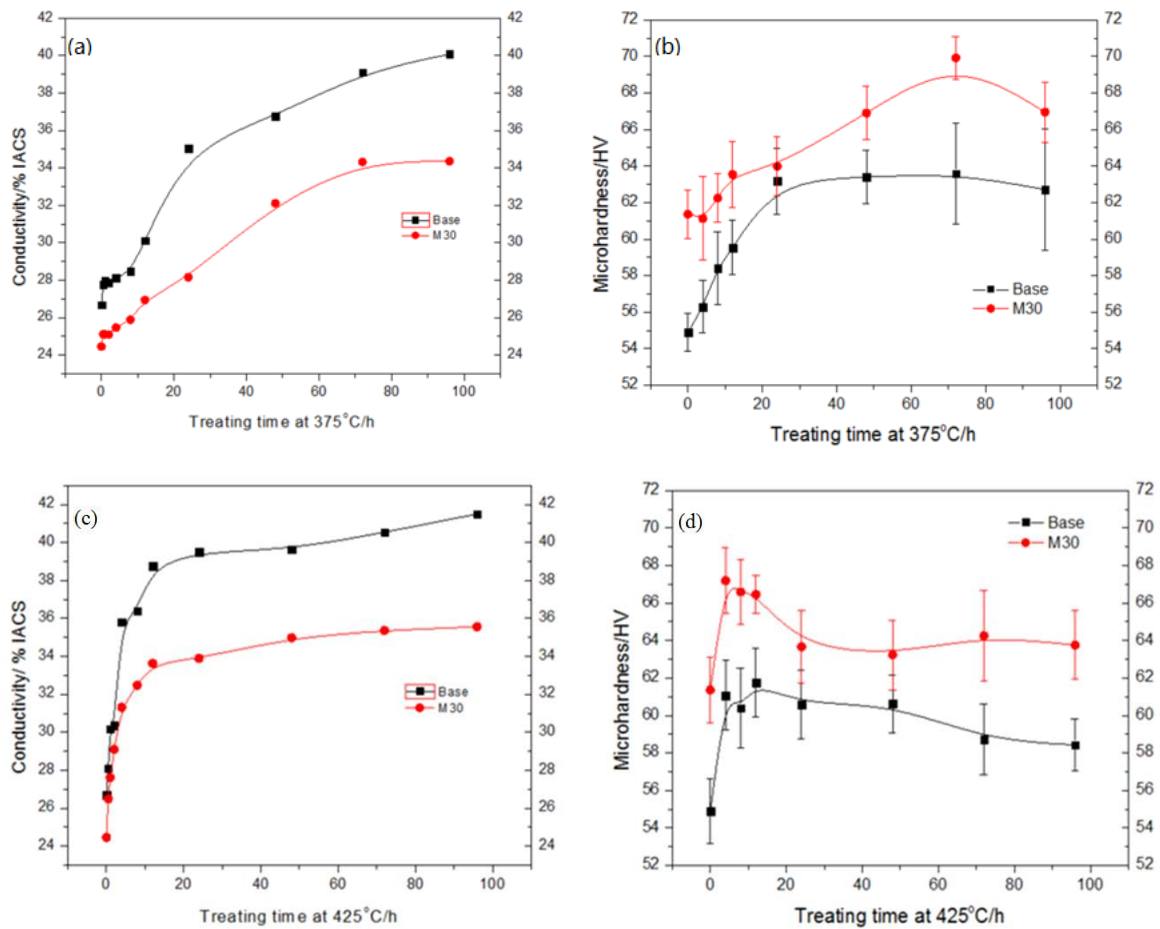


Fig. 4.16 Evolution of (a) electrical conductivity at 375°C; (b) microhardness at 375°C; (c) electrical conductivity at 425°C; (d) microhardness 425°C for Base 3004 and M30 alloys during precipitation treatment

Fig. 4.16 show the electrical conductivity and microhardness evolution for base 3004 alloy and M30 alloy during precipitation treatment at 375°C and 425°C. The results revealed the influence of the precipitation treatment temperature on the precipitation behaviour of dispersoids. As shown in Fig. 4.16a, the values of EC generally increased with increasing holding time, and reached the peak value after 96 hours for base 3004 and 72 hours for M30

alloy at 375°C. At higher temperature of 425°C (Fig. 4.16c), the EC rapidly increased and reached the peak value at around 12 hours and then increased slightly with increasing holding time. The evolution of the microhardness under these two temperatures also has big difference. For 375°C, the microhardness increased with increasing holding time, and reached the peak values after 48 hours for the base alloy and after 72 hours for M30 alloy, respectively. As for 425°C, the microhardness first increased significantly faster than at 375°C, and reached the maximum value after 12 hours and then slowly decreased with increasing holding time.

The evolution of microhardness can be attributed to the precipitation and coarsening of dispersoids during precipitation treatment. When the alloy was treated under 375°C, which is near the precipitation temperature of the α -Al(Mn,Fe)Si dispersoids, fine dispersoids were continuously precipitated and no significant coarsening occurred. After 48 hours treatment, the amount of the fine dispersoids reached the peak value and provided the maximum microhardness value for the alloy. As under 425°C, which is much higher than the precipitation temperature of α -Al(Mn,Fe)Si dispersoids, the growth rate of dispersoids is higher. The precipitation of α -Al(Mn,Fe)Si dispersoids was much faster, and the EC and microhardness reached the maximum value much earlier. After the peak values, the α -Al(Mn,Fe)Si dispersoids were coarsening with prolonged holding time, and the microhardness decreased with increasing time.

Compared with base 3004 alloy, M30 alloy possesses lower EC and higher microhardness under 375°C and 425°C. There is difference on the microhardness evolution tendency between base 3004 and M30 alloys. For 375°C, the microhardness and EC values of M30 reach the peak after around 72 hours, while base 3004 alloy is around 48 hours. For 425°C after 24 hours, the microhardness for the base alloy is gradually decreased because of the coarsening of the α -Al(Mn,Fe)Si dispersoids, while the microhardness for M30 alloy was quite stable. All these result indicated that the low diffusion rate of Mo could make the dispersoid coarsening slowly and keep their strengthening effect with extended treating time..

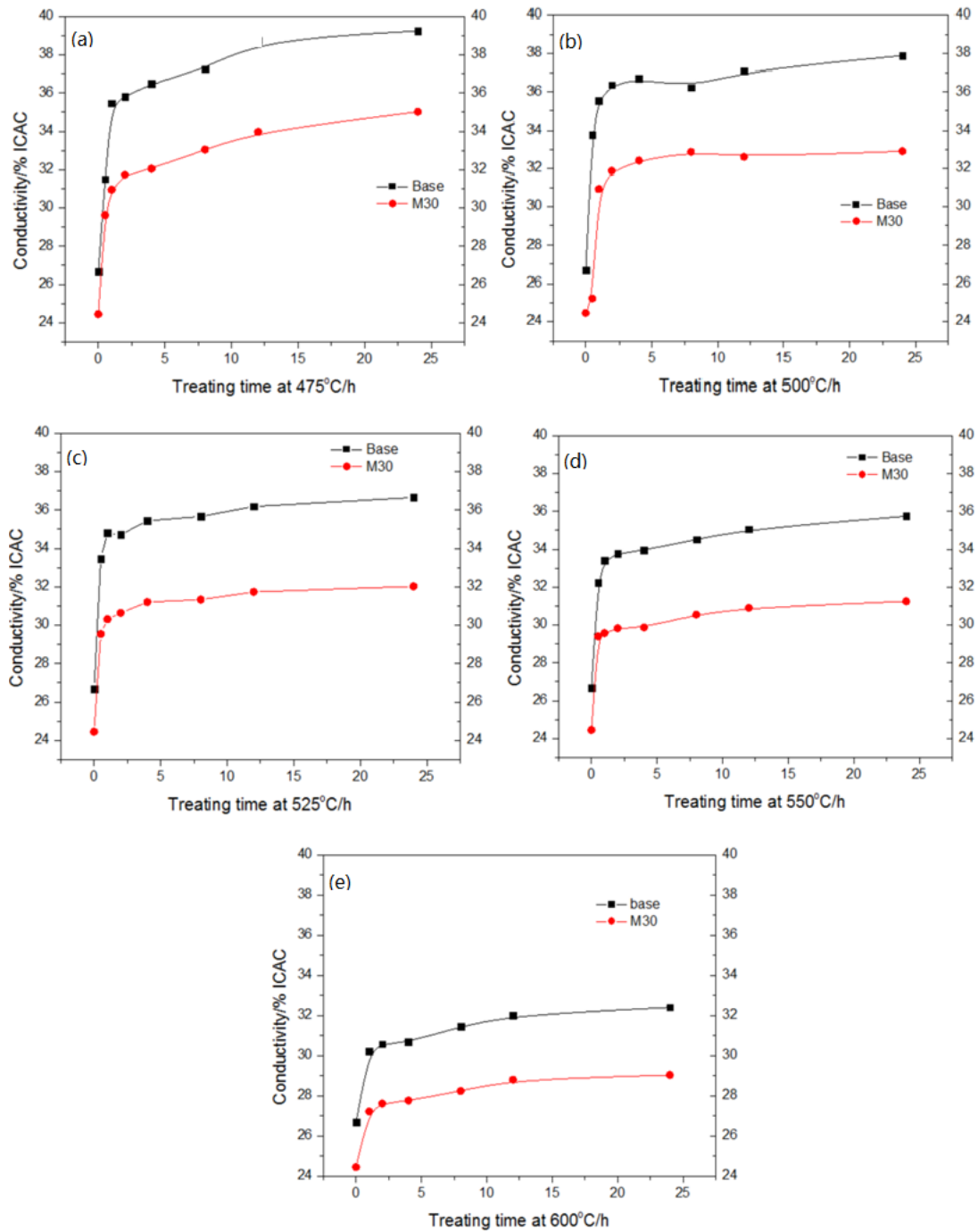


Fig. 4.17 Evolution of electrical conductivity for base 3004 and M30 alloys during precipitation treatment at different temperatures (a) 475°C, (b) 500°C, (c) 525°C, (d) 550°C, (e) 600°C

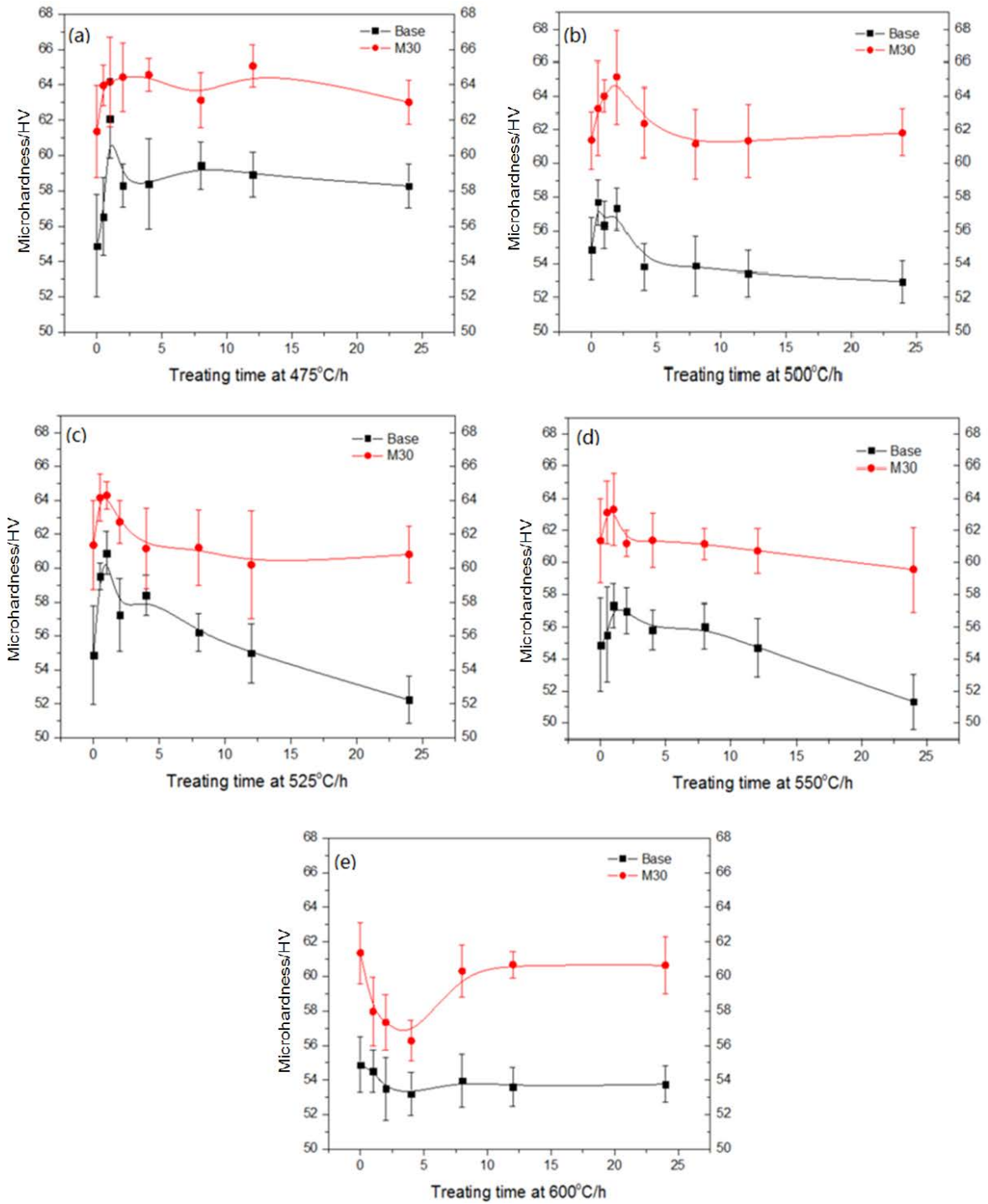


Fig. 4.18 Evolution of microhardness for base 3004 and M30 alloys during precipitation treatment at different temperatures (a) 475°C, (b) 500°C, (c) 525°C, (d) 550°C, (e) 600°C

Fig. 4.17 and Fig. 4.18 show the evolution of EC and microhardness for base 3004 alloy and M30 alloys during precipitation treatment at higher temperatures, ranged from 475°C to 600°C. The EC evolution at different precipitation temperature shows the similar tendency. Since all those precipitation temperature are quite high, the decomposition of Mn and Mo solid solution happened quickly and made the EC increased rapidly with the high diffusion rate of Mn and Mo. The EC quickly rose up within 1 hour during these precipitation treatments, and slowly increased with increasing holding time. But the maximum value of them are different because of different precipitation temperatures. With higher temperature, the solid solubility of Mn is higher, more Mn solute would stay in the Al matrix, causing lower EC. As for the influence of Mo content, M30 alloy always possess lower EC for all these precipitation treatment, independent on the precipitation temperature and time.

Microhardness evolution indicated that the Mo addition in AA3004 alloy has the solid solution strengthening effect and can improve the dispersion strengthening. During precipitation treatment at 475°C to 550°C, the microhardness of the alloys first increased with the precipitation of dispersoids. In general, the values of the microhardness reached the peak value within 1 or 2 hours. Then, the coarsening of the dispersoids led the decrease of the microhardness with the extended holding time. Higher precipitation temperature led quicker coarsening effect and made the microhardness drop faster. Comparing with base 3004 alloy, M30 alloy has higher and more stable microhardness with extending holding time at high

precipitation temperatures. The hardness drop caused by the coarsening dispersoids is significantly less in M30 alloy. For 600°C, because of the extremely high temperature, the dispersoids dissolved into the aluminum matrix after the precipitation and some Mn and Fe containing intermetallic particles also dissolved, and the solution levels of two alloys rose and the values of EC were lower than those at lower temperatures (475 to 550°C). Thus the microhardness decreased within first four hours treatment. After the partial dissolution of the dispersoids, the microhardness of the base alloy remained stable while the microhardness of M30 alloy slowly increased.

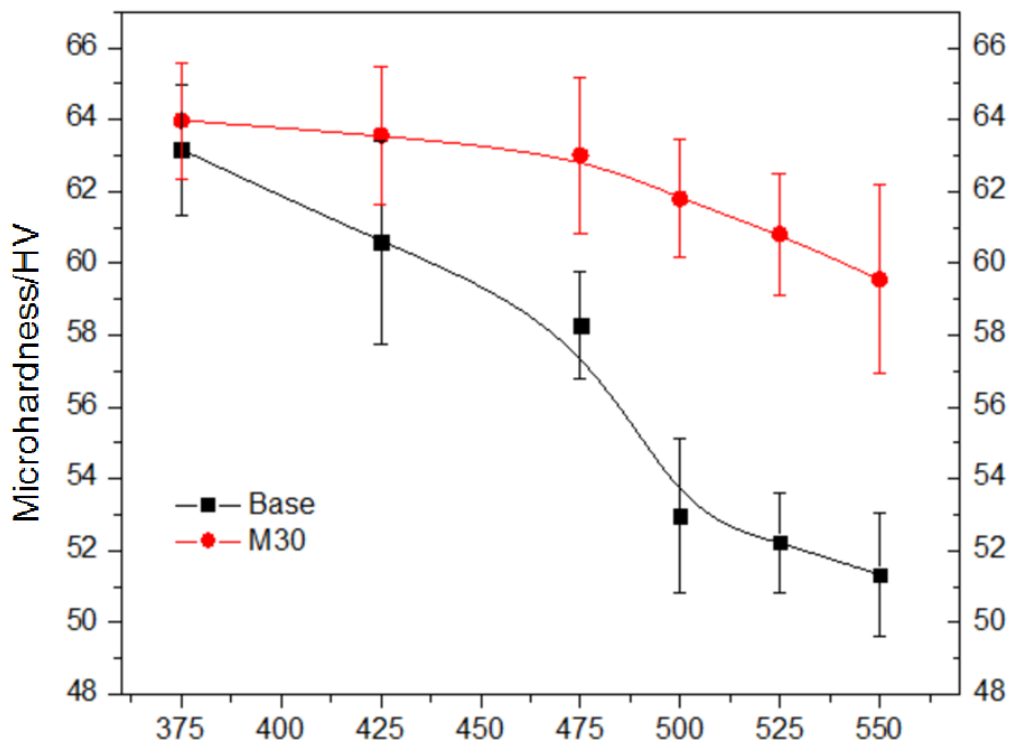


Fig. 4.19 Microhardness for base 3004 and M30 alloys after precipitation treatment for 24 hours at different temperature.

The microhardness results for base 3004 alloy and M30 alloy after precipitation treatment for 24 hours at different temperatures were shown in Fig. 4.19. The microhardness for base 3004 alloy decreases pretty quickly with increasing precipitation temperature. Base 3004 alloy has a high microhardness value 63HV after precipitation treatment at 375°C for 24 hours, while after precipitation treatment at 550°C for 24 hours, the microhardness remains only 51HV. The decrease of the microhardness is caused by the coarsening of dispersoids. After precipitation treatment at 375°C, base 3004 alloy can form a large amount of fine dispersoids with low DFZ. With increasing temperature, the increasing diffusion rate of Mn made the dispersoids coarsening faster. Thus, increasing precipitation temperature results in less amount and larger size of dispersoids as well as wider DFZ, causing the decrease of microhardness. However, the decrease of microhardness with increasing precipitation temperature is significantly less for M30 alloy because of the higher dispersoids coarsening resistance provided by Mo addition. With the temperature increased from 375°C to 550°C, the microhardness of M30 alloy only decreased from 64 HV to 60 HV.

The yield strength of base 3004 alloy and M30 alloy after different precipitation treatments at 24 hours was also tested at 300°C to evaluate their mechanical properties under elevated temperature and the result was shown in Fig. 4.20. The YS results showed a similar tendency with the microhardness results, the YS values at 300°C of M30 alloy are higher than the alloy at any precipitation temperature. The positive strengthening effects provided by Mo

can have great benefits for the applications at elevated temperature.

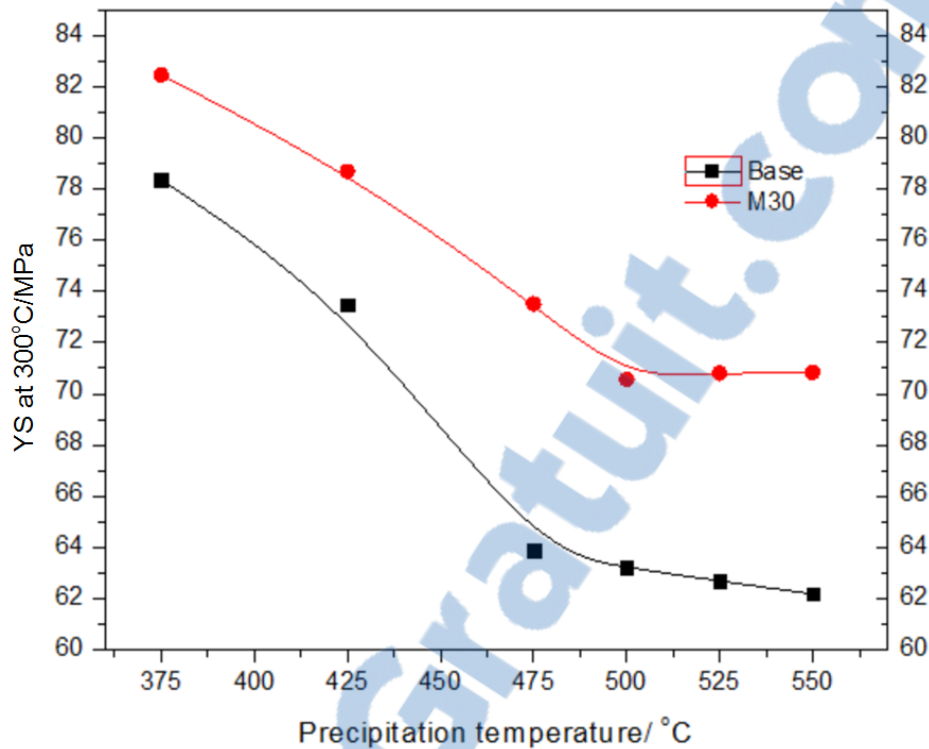


Fig. 4.20 Yield strength at 300°C for base 3004 and M30 alloys after precipitation treatment for 24 hours at different temperature

In order to thoroughly study the effect of Mo on dispersoids precipitation behavior, especially on retarding the coarsening rate of the dispersoids, a series of samples were treated under a combined procedure. Both base 3004 alloy and M30 alloy were first treated at 375°C for 48 hours to have the volume fraction of fine dispersoids as high as possible. Then, they were thermally held at 500°C up to 12 hours, in which the high temperature provided the favourable condition for the coarsening of the dispersoids. The microhardness and EC results are showed in Fig. 4.21. There is an increase of EC for both the base 3004 alloy and M30

alloy within the first two hours at 500°C, which indicated the additional precipitation of the dispersoids. Meanwhile the microhardness also increased for these two alloys. The microhardness of M30 alloy increased from 67HV to 69HV after 2 hours treatment at 500°C, then decreased with increasing holding time. The microhardness of base 3004 alloy slightly increased from 63HV to 64HV and decreased with increasing holding time. Although base 3004 alloy may precipitate few additional dispersoids at the beginning of the precipitation treatment at 500°C, the dispersoids coarsened also quickly because of the high temperature, and thus barely have any additional contribution on the microhardness. On the other hand, because of the Mo addition, the dispersoids in M30 alloy coarsened slower and have better strengthening effect. After 2 hours, the microhardness for base 3004 and M30 alloy decrease with increasing time.

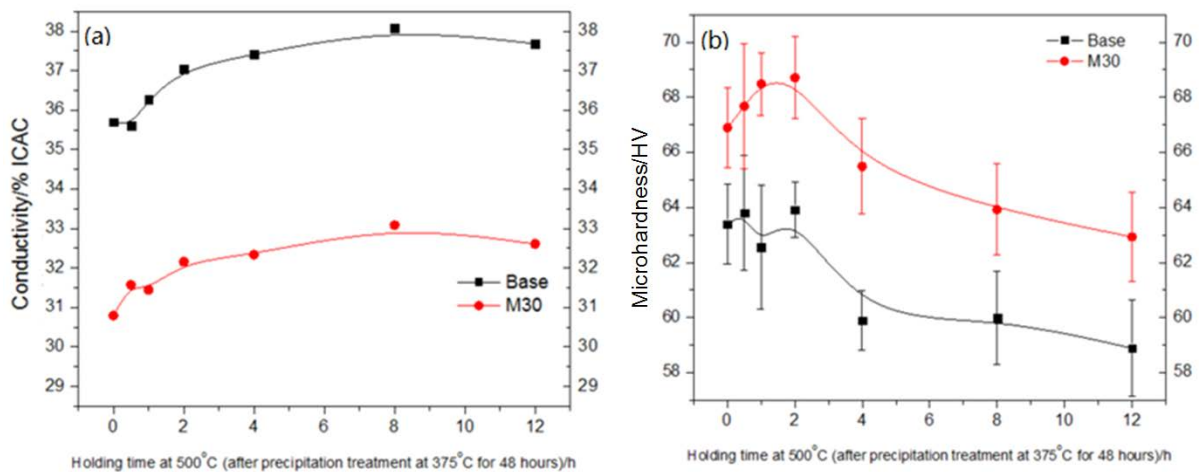


Fig. 4.21 (a)Electrical conductivity and (b) Microhardness evolution during the second step precipitation treatment at 500°C after the first precipitation treatment at 375°C for 48 hours

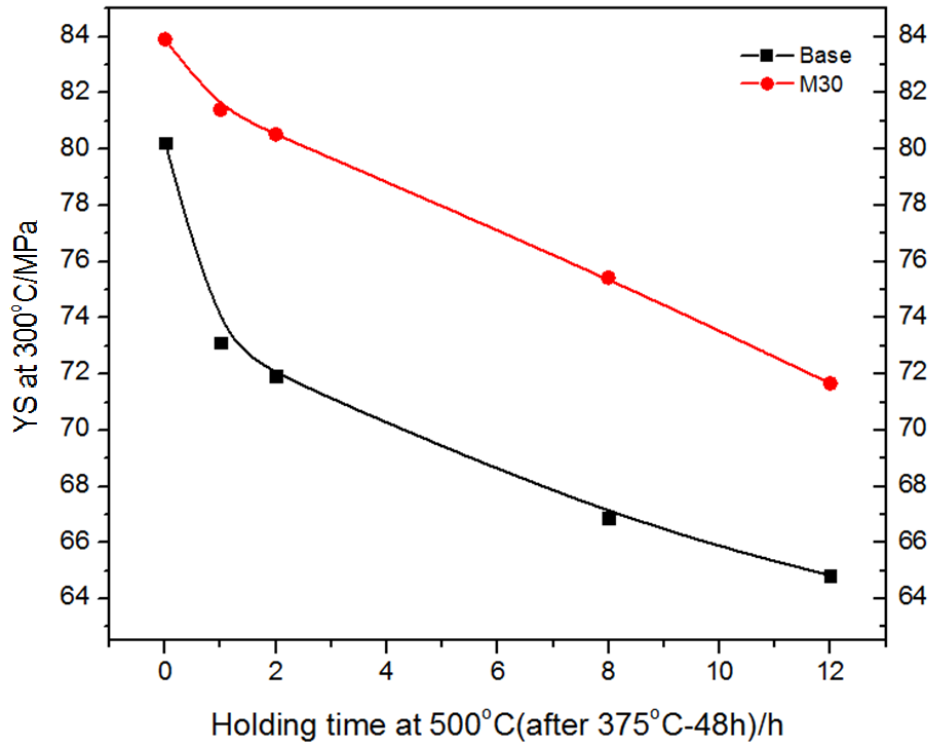


Fig. 4.22 Evolution of YS at 300°C during the second step precipitation treatment at 500°C after precipitation treatment at 375°C for 48 hours

The evolution of YS at 300°C (Fig. 4.22) indicates that Mo can provide better coarsening resistance for 3004 alloy. The YS for base 3004 alloy quickly dropped to 72 MPa from 80 MPa after first two hours at 500°C, while M30 alloy only slightly dropped to 81 MPa from 84 MPa. The better coarsening resistance by Mo addition makes M30 alloy more thermally stable in mechanical properties and provides the Mo contained alloys the great possibility even working as high as at 500°C for a short period.

4.3 Creep resistance and long-term thermal stability

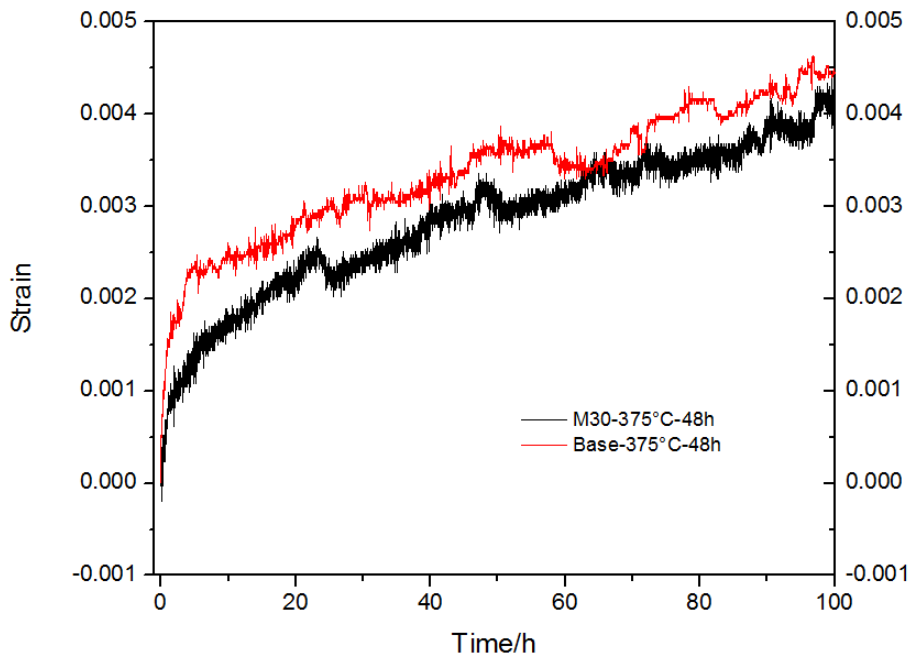


Fig. 4.23 Compressive creep curves at 300°C

The creep resistance of both base 3004 alloy and M30 alloy was investigated after the peak precipitation treatment(375°C/48h), the creep resistance curves were captured at 300°C under 45MPa for 100 hours. As shown in Fig. 4.23, base 3004 alloy and M30 alloy have a great creep resistance at 300°C, and after 100 hours holding, the total strain of creep deformation of these two alloys were lower than 0.005. Meanwhile, M30 alloy have even better creep resistance comparing with base 3004 alloy. During holding, the strain of M30 alloy is constantly lower than base 3004 alloy at fixed holding time. After 100 hours at 300°C, the total strain of M30 alloy is 0.0040 with creep rate of $1.11 \times 10^{-8} \text{s}^{-1}$, while the base 3004 alloy is 0.0045 with creep rate of $1.3 \times 10^{-8} \text{s}^{-1}$. The great creep resistance for these two

experiment alloys is contributed by the fine and uniformly distributed dispersoids after the peak precipitation treatment. The dislocations in the aluminum matrix were pinned by the thermally stabilized dispersoids, resulting a great creep resistance at 300°C. Moreover, the better creep resistance of M30 alloy may attribute to the additional solid solution strengthening and finer dispersoids in the matrix by Mo addition.

The recent work of Liu et al[11] has showed that 3004 alloys possess great thermal stability during long-term holding at 300°C. In order to further investigate the long-term thermal stability of the dispersoids, as well as the influence of Mo addition, the M30 alloy and Base alloy after the peak precipitation treatment(375°C/48h) were held at 350°C and 400°C for up to 1000 hours.

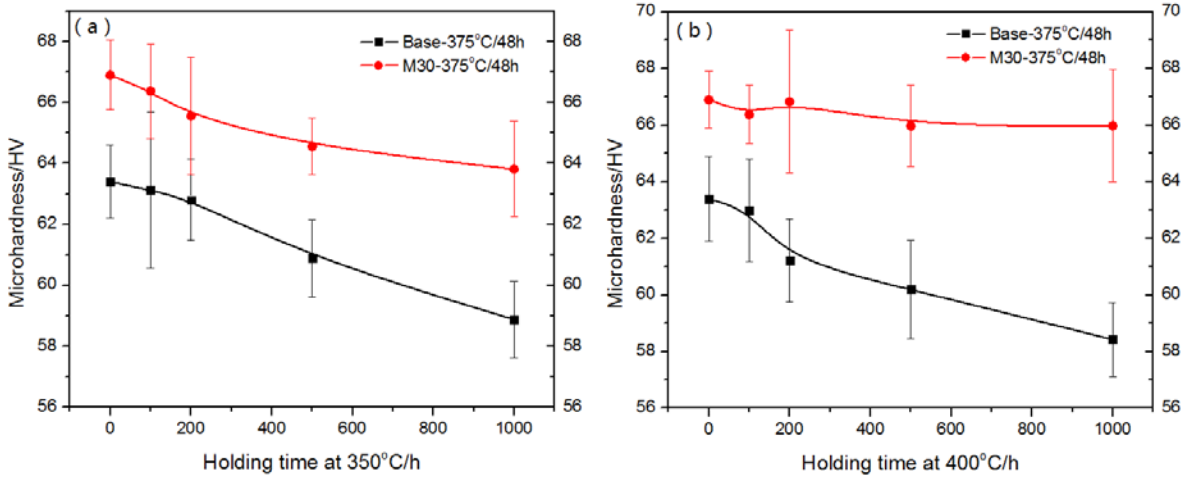


Fig. 4.24 Microhardness evolution during long thermal holding at different temperature (a) 350°C; (b)

400°C

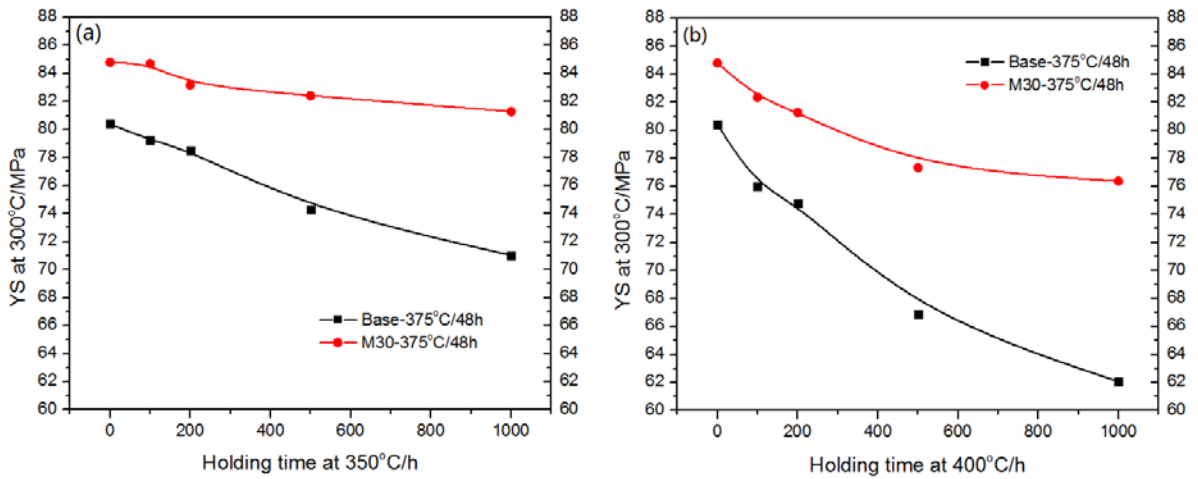


Fig. 4.25 Evolution of YS at 300°C during long thermal holding at different temperature (a) 350°C; (b)

400°C

After the thermal holding, the microhardness were tested, the result is in Fig. 4.24, after long thermal holding at 350°C and 400°C, the microhardness of M30 alloy is more stable compared with base 3004 alloy. Meanwhile, the YS at 300°C were tested, the result is shown in Fig. 4.25. After holding at 350°C for 1000h, the YS at 300°C of M30 alloy is quite stable

and the value of YS is still above 80MPa. However, for the base alloy, the YS decreases more obviously with the increasing holding time. After 1000 hours at 350°C, the YS of M30 alloy only declined from 85MPa to 81MPa, while the YS of base 3004 alloy declined from 81MPa to 71MPa. When the holding temperature is higher (at 400°C), the deterioration of the YS is faster, but M30 alloy still has more stabilized YS values compared with base 3004 alloy. As shown in Fig. 4.25b after holding at 400°C for 1000 hours, the YS of base 3004 alloy declined from 81MPa to 62MPa, while M30 alloy only declined from 85MPa to 76MPa. The YS at higher temperature after long thermal holding(Fig. 4.26) also revealed the similar tendency. The YS of M30 alloy is significantly more stable than base 3004 alloy while tested at 350°C and 400°C, after 1000h holding, M30 alloy possessed evidently higher YS.

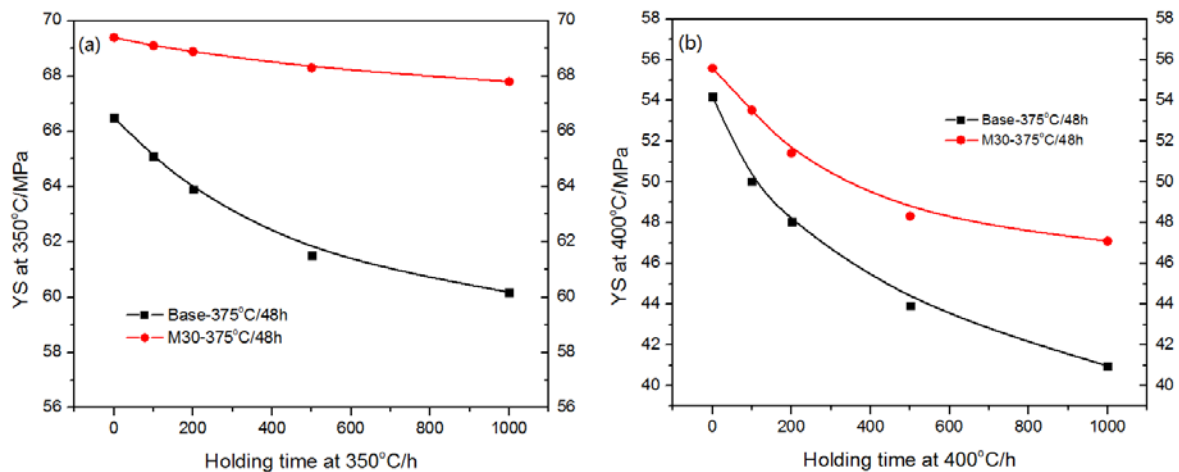


Fig. 4.26 Evolution of YS during long thermal holding at different temperature holding and tested at (a) 350°C; (b) 400°C

The significant improvement of long-term thermal stability for M30 alloy is contributed

by the excellent dispersoid coarsening resistance that provided by the Mo addition. Results of holding at 350 and 400°C confirmed that the Mo-containing α -Al(Mn,Fe,Mo)Si dispersoids have better coarsening resistance than α -Al(Mn,Fe)Si dispersoids in the base alloy, which help the dispersoids maintain fine size and continuously provide strengthening effect at high temperature. The better thermal stability of mechanical properties provided by Mo addition opens a wider opportunities for AA3004 alloys in high temperature applications.

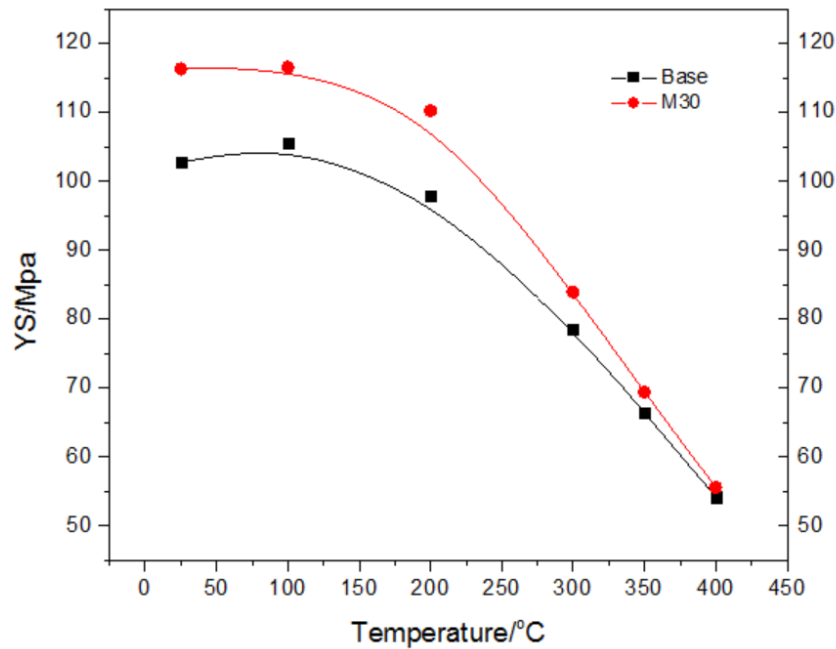


Fig. 4.27 Evolution of YS at different temperature after peak precipitation treatment(375°C/48h)

The YS (with zero hold time) at different temperatures after peak precipitation treatment (375°C/48h) was tested for both M30 and base 3004 alloy (Fig. 4.27). The YS for the alloys were quite stable when the temperature is not higher than 200°C, the YS of base alloy is higher than 95MPa at the temperature region from 25-200°C, while the YS of M30 alloy is

around 110MPa. When the temperature is higher than 200°C, the YS started to decrease. When the temperature reaches 400°C, the YS of base 3004 and M30 alloy both decreased to around 55MPa. After the peak precipitation treatment (375°C/48h), M30 alloy possesses a higher YS (116MPa) than Base 3004 alloy (102MPa) the temperature range of 25-200°C, which is contribute by the fine size of α -Al(Mn,Fe,Mo)Si dispersoids. When the temperature increases, the difference of YS between these two alloys becomes narrowed, but M30 alloy always has higher YS within the temperature region from 200 to 400°C, attributed to the better coarsening resistance of Mo-containing α -Al(Mn,Fe,Mo)Si dispersoids.

4.4 Preheating treatment

The dispersion strengthening effect in aluminum alloys is highly related to the size and distribution of dispersoids particles. A larger volume of finer dispersoids in aluminum matrix can provide better strengthening effect. Recent research showed that proper multi-step heat treatment can improve the distribution of dispersoids in aluminum alloys[41-44]. Multi-step heat treatment applies one or two additional low temperature heat treatment before the conventional precipitation treatment to create a favourable condition of dispersoids precipitation and develop a desirable distribution.

In the current study, three groups of preheating precipitation treatment at different temperatures from 175°C, 250°C and 330°C were designed (Table 3.2). The preheating treatment was applied a low temperature treatment before the precipitation treatment at 375°C for 48 hours. Based on the previous results in this research, both of the base 3004 alloy and M30 alloy can form a large volume of fine dispersoids after precipitation treatment at 375°C for 48 hours. It is expected that the strengthening effect can still be improved by getting more optimized dispersoids distribution.

Recent literature reported that the formation of Mg_2Si could be the potential nuclei of $\alpha-Al(Mn,Fe)Si$ dispersoids[45], and the two step heat treatment can provide both a finer particle size and higher number density of dispersoids in aluminum alloy[41]. The preheating

precipitation treatment was applied for base 3004 alloy first, the microhardness for base 3004 alloy were tested after the second step precipitation treatment, the results were showed in Fig. 4.28. For 175°C, the microhardness slightly increased after 4 hours treatment, then decreased with increasing time, after 24 hours pretreatment the hardness is lower than the original peak precipitation state. For 250°C the microhardness for Base 3004 alloy continuously increased with increasing time and get the peak value after 24 hours treatment. The increase is quite considerable, from 63HV to 69HV and the tendency is pretty obvious. As for 330°C, there was an slight increase of microhardness, after 48 hours treatment the microhardness increased from 63HV to 66HV.

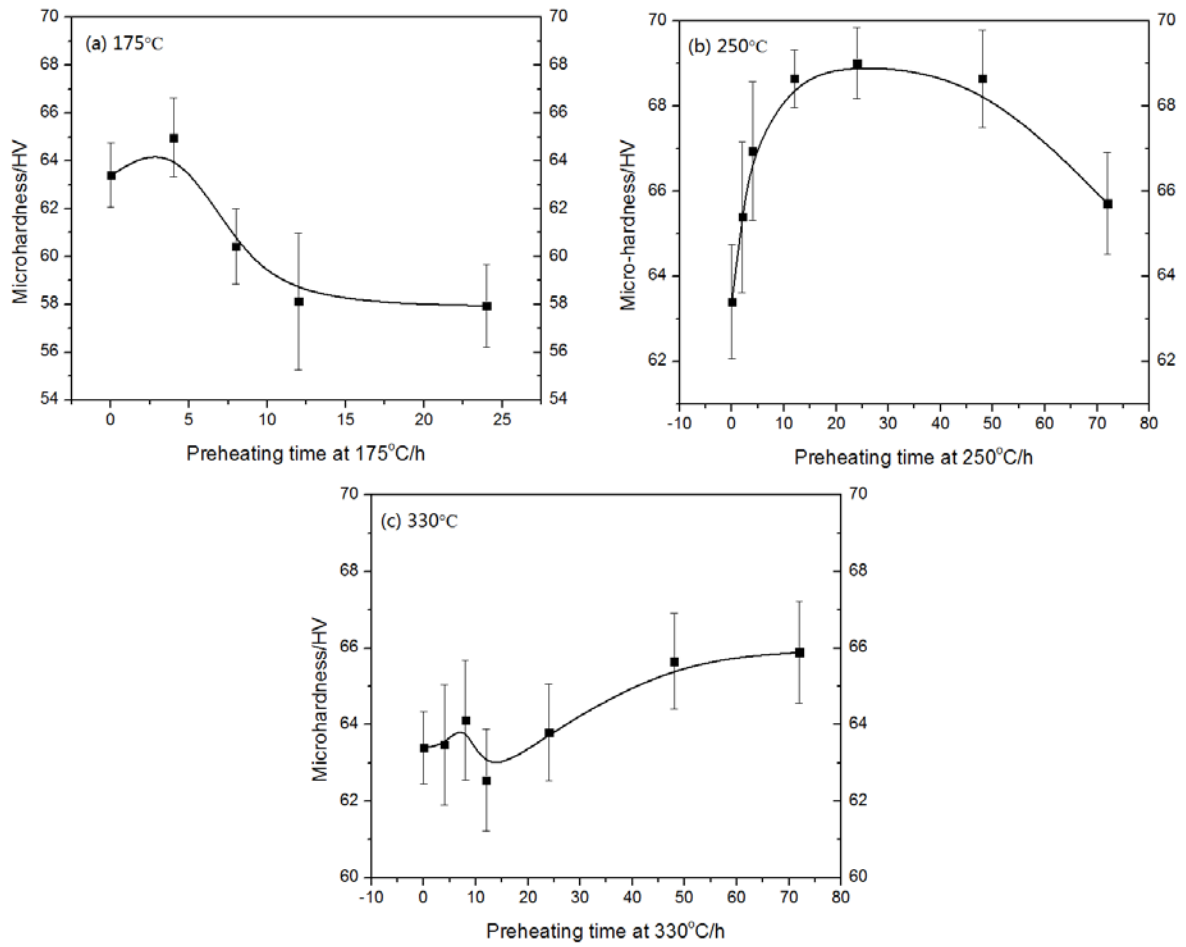


Fig. 4.28 The microhardness for different holding times during the first step precipitation treatment at (a) 175°C, (b) 250°C and (c) 330°C

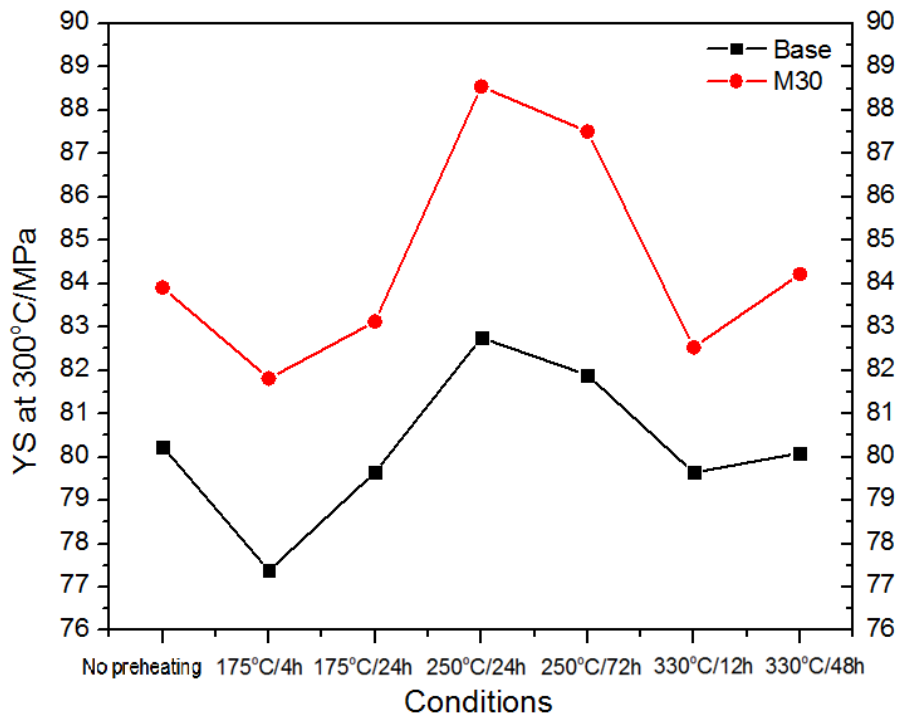


Fig. 4.29 YS at 300°C for different preheating treatment.

Furthermore, the yield strength at 300°C of base 3004 and M30 for both three group preheating precipitation treatment were tested with selected two condition in each group, and the result is showed in Fig. 4.29. The tendency for base 3004 and M30 alloy are similar. For 175°C and 330°C, with the additional preheating, the YS at 300°C was slightly decreased, but the result for 250°C is quite promising. The YS increased with additional preheating at 250°C, especially with 24 hours treatment. The value of YS increased from 80Mpa to 83Mpa for base 3004 alloy, and from 84Mpa to 88Mpa for M30 alloy. Meanwhile, the long-term thermal holding results (Fig. 4.30) revealed that additional preheating at 250°C for 24 hours can improve the YS at 300°C of AA3004 alloy after long-term holding, showing a better



long-term thermal stability.

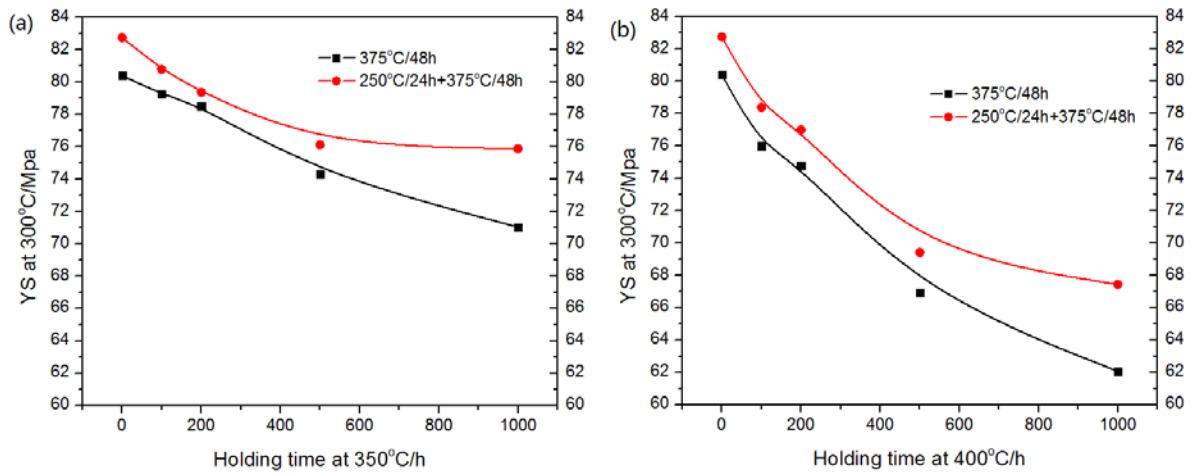


Fig. 4.30 Long-term thermal holding results (a) at 350°C (b) at 400°C

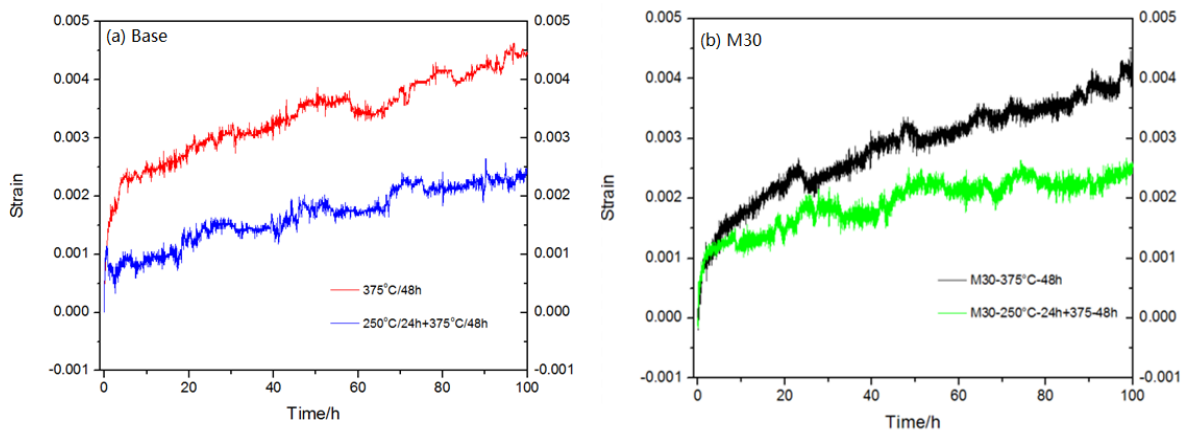


Fig. 4.31 Compressive creep curves at 300°C for (a)base 3004 alloy, (b) M30 alloy with preheating at 250°C

Furthermore, the creep resistance of the base 3004 alloy and M30 alloy with preheating at 250°C was tested at 300°C(Fig. 4.31), the result revealed a great improvement on creep resistance. With additional preheating at 250°C for 24 hours, the total creep strain for base 3004 alloy and M30 alloy are improved significantly. After the peak precipitation treatment(375°C/48h) the strain was reduced from 0.0044 to 0.0022, which is 50% less. And

the creep was reduced from $1.3 \times 10^{-8} \text{s}^{-1}$ to $6.1 \times 10^{-9} \text{s}^{-1}$. The improvement of creep resistance is contributed by the more and finer dispersoids provided by the preheating treatment. The dispersoids can effectively pin the dislocations and hinder the glide and climbed of them, resulting a better creep resistance.

5. Conclusions

- (1) The as-cast microstructure is similar with the base 3004 alloy with the addition of Mo up to 0.3 wt.%, which is consist of $\text{Al}_6(\text{MnFe})$, $\alpha\text{-Al}(\text{MnFe})\text{Si}$ and Mg_2Si intermetallics and almost all the Mo is soluted in the matrix while little Mo-containing intermetallics are detected. However, the Mo-containing primary intermetallics begin to form when the addition of Mo is higher than 0.4 wt.%, which is hard to be dissolved during the homogenization at 600°C .
- (2) The solid solution hardening of Mo leads to the increase of as-cast microhardness with the addition of Mo until to the peak value at 0.3-0.4 wt.% followed by the gradual decrease with further increasing Mo content.
- (3) During the precipitation treatment ($375^\circ\text{C}/48\text{h}$), the $\alpha\text{-Al}(\text{MnFeMo})\text{Si}$ dispersoids can form both interdendrite and intradendrite, which results in the increase of the volume fraction of dispersoids and the decrease of the dispersoid free zone (DFZ) compared with the base 3004 alloy.

- (4) The microhardness and yield strength at 300°C increases with increasing Mo addition from 0 to 0.3 wt. % after precipitation treatment (375°C/48h), confirming the positive contribution of Mo on improving the properties of 3004 alloys.
- (5) Under the precipitation treatment, the microhardness and yield strength increase with increasing time to a peak followed by a plateau (<475°C) or a gradual decrease (>475°C) in Mo-containing alloys. The microhardness and strength slowly decrease with increasing temperature at fixed time. However, the properties at high temperatures are higher with lower decreasing rate in Mo-containing alloys compared with the base alloy.
- (6) The creep resistance has been further improved in Mo-containing alloys due to the uniformly distributed dispersoids at higher volume fraction and less dispersoids free zone.
- (7) Compared with the base alloy, the microhardness and yield strength exhibit more stable at 350°C in Mo-containing alloys. However, it gradually reduces when holding at 400°C but the decreasing rate is much lower than that of the base alloy.
- (8) Additional pretreatment at 250°C for 24 hours followed by the peak precipitation treatment (370°C for 24-48 hours) can further improve the strength and creep resistance in both base 3004 and Mo-containing alloys.
- (9) With the pretreatment at 250°C for 24 hours for the 0.3 wt.% Mo containing alloy, the yield strength and creep resistance at 300°C can be further improved by 12% (from 78MPa to 88MPa) and 53% (from $1.3 \times 10^{-8} \text{s}^{-1}$ to $6.1 \times 10^{-9} \text{s}^{-1}$ in minimum creep rate),

respectively, compared with the base 3004 alloy after peak precipitation treatment.

Reference

- [1] R. Nunes, ASM Handbook volume2:properties and selection:nonferrous alloys and special-purpose materials, 1990.
- [2] G. E.Totten, Handbook of aluminum, 2003.
- [3] J.G. Kaufman, Properties of aluminum alloys : tensile, creep, and fatigue data at high and low temperatures, ASM International ; Aluminum Association, Materials Park, Ohio; Washington, D.C., 1999.
- [4] I.J. Polmear, M.J. Couper, Metall. Trans. A, 19 (1988) 1027-1035.
- [5] Y.J. Li, L. Arnberg, Acta Materialia, 51 (2003) 3415-3428.
- [6] D. Alexander, A. Greer, Acta Materialia, 50 (2002) 2571-2583.
- [7] M. Warmuzek, G. Mrówka, J. Sieniawski, Journal of Materials Processing Technology, 157-158 (2004) 624-632.
- [8] S. Ding, J. Qiu, J. G.Morris, The Minerals, Metals & Materials Society, (1998) 39-48.
- [9] Y.J. Li, A.M.F. Muggerud, A. Olsen, T. Furu, Acta Materialia, 60 (2012) 1004-1014.
- [10] A.M.F. Muggerud, E.A. Mørtzell, Y. Li, R. Holmestad, Materials Science and Engineering: A, 567 (2013) 21-28.
- [11] K. Liu, X.G. Chen, Materials & Design, 84 (2015) 340-350.
- [12] Y.J. Li, L. Arnberg, Precipitation of dispersoids in DC-CAST AA3103 alloy during heat treatment, in: P.N. Crepeau (Ed.) Light Metals 2003, Minerals, Metals & Materials Soc, Warrendale, 2003, pp. 991-997.
- [13] H.-W. Huang, B.-L. Ou, Materials & Design, 30 (2009) 2685-2692.
- [14] A.M.F. Muggerud, Y. Li, R. Holmestad, Philosophical Magazine, 94 (2014) 556-568.
- [15] A.M.F. Muggerud, Y.J. Li, R. Holmestad, Materials Science Forum, Trans Tech Publ, 2014, pp. 39-44.
- [16] Y.J. Li, L. Arnberg, Acta Mater., 51 (2003) 3415-3428.
- [17] Y.J. Li, A.M.F. Muggerud, A. Olsen, T. Furu, Acta Mater., 60 (2012) 1004-1014.
- [18] Y. Li, L. Arnberg, Precipitation of Dispersoids in DC-Cast AA3103 Alloy during Heat Treatment, Essential Readings in Light Metals, John Wiley and Sons, 2013, pp. 1021-1027.
- [19] E. Nes, Scr. Metall., 10 (1976) 1025-1028.
- [20] E. Nes, Acta Metall., 24 (1976) 391-398.
- [21] A.M.F. Muggerud, Y.J. Li, R. Holmestad, 14th International Conference on Aluminium Alloys, ICAA 2014, Trans Tech Publications Ltd, Trondheim, 2014, pp. 39-44.
- [22] Q. Du, W.J. Poole, M.A. Wells, N.C. Parson, Acta Materialia, 61 (2013) 4961-4973.
- [23] A.R. Farkoosh, X. Grant Chen, M. Pekguleryuz, Materials Science and Engineering: A, 620 (2015) 181-189.
- [24] A.R. Farkoosh, X. Grant Chen, M. Pekguleryuz, Materials Science and Engineering: A, 627 (2015) 127-138.
- [25] I.J.Polmear, M.J.Couper, Design and development of an experimental wrought aluminum alloy for use at elevated temperatures, Metallurgical Transaction A, 1988, pp. 1027-1035.
- [26] L. Lodgaard, N. Ryum, Materials science and technology, 16 (2000) 599-604.
- [27] U. PRAKASH, T. RAGHU, A.A. GOKHALE, S.V. KAMAT, JOURNAL OF MATERIALS SCIENCE, 34 (1999) 5061 – 5065.
- [28] E.A. MARQUIS, D.N. SEIDMAN, Acta Materialia, 49 (2001) (2001) 49 (2001) 1909–1919.
- [29] T. Rouns, Aluminum Alloys for Packaging III, TMS, (1998) 3-20.

- [30] Y.J. Li, L. Arnberg, *Materials Science and Engineering*, A347 (2003) (2003) 130 /135.
- [31] M. Dehmas, E. Aeby-Gautier, P. Archambault, M. Serrière, *Metallurgical and Materials Transactions A*, 44 (2012) 1059-1073.
- [32] D.T.L. Alexander, A.L. Greer, *Acta Materialia*, 50 (2002) 2571-2583.
- [33] H. Merchant, J. Morris, D. Hodgson, *Materials Characterization*, 25 (1990) 339-373.
- [34] E. Nes, *Acta Metallurgica*, 24 (1976) 391-398.
- [35] F. Humphreys, *Acta Metallurgica*, 25 (1977) 1323-1344.
- [36] K. Knipling, *Acta Materialia*, 56 (2008) 1182-1195.
- [37] B. Forbord, H. Hallem, J. Røyset, K. Marthinsen, *Materials Science and Engineering: A*, 475 (2008) 241-248.
- [38] Q. Zhao, B. Holmedal, Y. Li, *Philos. Mag.*, 93 (2013) 2995-3011.
- [39] C. Kuehmann, P. Voorhees, *Metallurgical and Materials Transactions A*, 27 (1996) 937-943.
- [40] K.E. Knipling, D.C. Dunand, D.N. Seidman, *Zeitschrift für Metallkunde*, 97 (2006) 246-265.
- [41] Z. Guo, G. Zhao, X.G. Chen, *Materials Characterization*, 102 (2015) 122-130.
- [42] Z. Jia, G. Hu, B. Forbord, J.K. Solberg, *Materials Science and Engineering: A*, 483-484 (2008) 195-198.
- [43] X.-y. Lü, E.-j. Guo, P. Rometsch, L.-j. Wang, *Transactions of Nonferrous Metals Society of China*, 22 (2012) 2645-2651.
- [44] Y.-l. Deng, Y.-y. Zhang, L. Wan, A.A. Zhu, X.-m. Zhang, *Metallurgical and Materials Transactions A*, 44 (2013) 2470-2477.
- [45] L. Lodgaard, N. Ryum, *Materials Science and Engineering A*, A283 (2000) 144–152.